Quantum phase transitions beyond Landau-Ginzburg theory in one-dimensional space revisited

Christopher Mudry,[1,2] Akira Furusaki,[3,4] Takahiro Morimoto,[5,6] and Toshiya Hikihara[7]
[1]*Condensed Matter Theory Group, Paul Scherrer Institute, CH-5232 Villigen PSI, Switzerland*
[2]*Institute of Physics, École Polytechnique Fédéerale de Lausanne (EPFL), CH-1015 Lausanne, Switzerland*
[3]*Condensed Matter Theory Laboratory, RIKEN, Wako, Saitama 351-0198, Japan*
[4]*RIKEN Center for Emergent Matter Science (CEMS), Wako, Saitama 351-0198, Japan*
[5]*Department of Physics, University of California, Berkeley, California 94720, USA*
[6]*Materials Science Division, Lawrence Berkeley National Laboratory, Berkeley, California 94720, USA*
[7]*Faculty of Science and Technology, Gunma University, Kiryu 376-8515, Japan*

(Received 27 March 2019; published 29 May 2019)

The phase diagram of the quantum spin-$\frac{1}{2}$ antiferromagnetic J_1-J_2 XXZ chain was obtained by Haldane using bosonization techniques [Haldane, Phys. Rev. B **25**, 4925 (1982); **26**, 5257 (1982)]. It supports three distinct phases for $0 \leqslant J_2/J_1 < \frac{1}{2}$, i.e., a gapless algebraic spin-liquid phase, a gapped long-range ordered Neel phase, and a gapped long-range ordered dimer phase. Even though the Neel and dimer phases are not related hierarchically by a pattern of symmetry breaking, it was shown that they meet along a line of quantum critical points with a U(1) symmetry and central charge $c = 1$. Here, we extend the analysis made by Haldane on the quantum spin-$\frac{1}{2}$ antiferromagnetic J_1-J_2 XYZ chain using both bosonization and numerical techniques. We show that there are three Neel phases and the dimer phase that are separated from each other by six planes of phase boundaries realizing Gaussian criticality when $0 \leqslant J_2/J_1 < \frac{1}{2}$. We also show that each long-range ordered phase harbors topological point defects (domain walls) that are dual to those across the phase boundary in that a defect in one ordered phase locally binds the other type of order around its core. By using the bosonization approach, we identify the critical theory that describes simultaneous proliferation of these dual point defects, and show that it supports an emergent U(1) symmetry that originates from the discrete symmetries of the XYZ model. To confirm this numerically, we perform exact diagonalization and density-matrix renormalization-group calculations and show that the critical theory is characterized by the central charge $c = 1$ with critical exponents that are consistent with those obtained from the bosonization approach. Furthermore, we generalize the field-theoretic description of direct continuous phase transition to higher dimensions, especially in $d = 3$, by using a nonlinear sigma model (NLSM) with a topological term. In particular, we propose the π-flux phase on the cubic lattice with local quartic interactions as a platform for direct continuous phase transition and deconfined criticality. We discuss possible phase diagrams for the π-flux phase on the cubic lattice with these quartic interactions from the renormalization flow of NLSMs.

DOI: 10.1103/PhysRevB.99.205153

I. INTRODUCTION

A paradigm for a phase transition with spontaneous symmetry breaking is the antiferromagnetic phase transition of quantum spin systems with antiferromagnetic exchange interactions. The antiferromagnetic phase is characterized by a local order parameter, the staggered magnetization. In dimensions above the lower critical dimension, it is sufficient to account for the smooth fluctuations of the order parameter, the spin waves, in order to describe the second-order transition from the antiferromagnetic to the paramagnetic phase.

The discovery of the Berezinskii-Kosterlitz-Thouless transition [1–4] demonstrated that fluctuations that are pointwise singular can also drive classical continuous phase transitions, while the spin waves are only good enough to downgrade long-range order to quasi-long-range order owing to the low dimensionality of space. In the context of quantum phase transitions, Haldane in Ref. [5] and Read and Sachdev in Ref. [6] pointed out that the proliferation of hedgehog defects in $(2 + 1)$-dimensional space-time have the potential to drive a transition from an antiferromagnetic ground state to a spin-dimerized ground state in spin-$\frac{1}{2}$ two-dimensional (2D) systems. Because both phases spontaneously break distinct symmetries of the microscopic Hamiltonian [the spin SU(2) symmetry in the antiferromagnetic phase and the point-group symmetry of the lattice in the spin-dimerized phase], such a transition was originally considered to be nongeneric and discontinuous.

This interpretation, derived as it is from the conventional wisdom based on the Landau-Ginzburg paradigm for symmetry breaking, was questioned in a series of theoretical papers [7–11], where it was proposed that a direct continuous quantum phase transition between the antiferromagnetic and spin-dimerized (valence bond solid) phases of 2D spin-$\frac{1}{2}$ systems is generic when driven by the proliferation of nontrivial point defects. In this scenario, the nature of the transition is encoded by the duality relating the point defects in the two phases. Namely, a point defect in one phase binds the order of the other phase in its core. At the transition, both types of point defects proliferate. It was also argued that the

critical theory is described by a doublet of bosonic matter fields that are coupled to a noncompact U(1) gauge field. This emerging scalar quantum electrodynamics is in its deconfined Coulomb phase and, hence, was called deconfined quantum criticality [7].

A series of numerical studies of 2D lattice models that were designed with the potential to host deconfined quantum criticality have been performed [12–24]. However, confirming numerically the existence of deconfined quantum criticality has been a hard task. First, one must identify the proper two-dimensional lattice model that may host a direct continuous quantum phase transition between two phases that break spontaneously and in distinct ways the symmetries of the lattice Hamiltonian. Second, the numerics must rule out a quantum phase transition that is weakly discontinuous.

Whereas the original proposal for deconfined quantum criticality referred to a direct phase transition between antiferromagnetic order and valence bond (dimerization) order, one may consider many-body quantum systems that are not quantum magnets, one may consider different choices of the ordered phases, and one may work in spaces with a dimensionality other than two [10,11,25–34]. In particular, if one considers discrete symmetries instead of continuous ones, one may seek examples of deconfined quantum criticality characterizing one-dimensional (1D) lattice Hamiltonians. This approach has recently been advocated in Ref. [35] in the context of quantum spin-$\frac{1}{2}$ chains.

In this paper, we report analytical and numerical studies of quantum spin-$\frac{1}{2}$ chains supporting the core idea of quantum criticality beyond the Landau-Ginzburg paradigm, namely, that a direct continuous quantum phase transition between two ordered phases can be interpreted as the proliferation of point defects that nucleate the order across the transition. Specifically, we identify the critical theory in $(1+1)$-dimensional space-time by the bosonization approach and show that the critical theory supports an emergent U(1) symmetry. Performing exact diagonalization and density-matrix renormalization-group (DMRG) calculations, we numerically confirm that the critical theory is characterized by the central charge $c = 1$ with critical exponents that are consistent with those from the bosonization approach.

We also argue that higher-dimensional analogs of deconfined quantum criticality can be obtained from fermionic tight-binding Hamiltonians that support a Dirac semimetallic phase with certain contact interactions. Mean-field decoupling of interactions naturally leads to a nonlinear sigma model (NLSM) augmented by a topological term. This topological term describes the mutual relationship between the defects in the two ordered phases and is responsible for deconfined quantum criticality. As an example in three-dimensional (3D) space, we demonstrate that the π-flux phase on the cubic lattice with contact interactions gives a natural platform for a duality between point defects that nucleate the antiferromagnetic (dimer) order at the core in the dimer (antiferromagnetic) phase.

The paper is organized as follows. The case of 1D space, $d = 1$, is treated in Sec. II. The case of 3D space, $d = 3$, is treated in Sec. III. A summary is given in Sec. IV.

II. J_1-J_2 XYZ MODEL ON A (LINEAR) CHAIN

A. Symmetries and phases

The sites of a spin chain are denoted by the letter $l = 1, \ldots, L$, where the number of sites L is assumed to be an even integer. We study the quantum spin-$\frac{1}{2}$ XYZ chain with the antiferromagnetic nearest-neighbor $J_1 > 0$ and next-nearest-neighbor $J_2 \geqslant 0$ couplings defined by the Hamiltonian

$$H := J_1 \sum_{l=1}^{L} \left(S_l^x S_{l+1}^x + \Delta_y S_l^y S_{l+1}^y + \Delta_z S_l^z S_{l+1}^z \right) + J_2 \sum_{l=1}^{L} \left(S_l^x S_{l+2}^x + \Delta_y S_l^y S_{l+2}^y + \Delta_z S_l^z S_{l+2}^z \right), \quad (2.1a)$$

where we have chosen to impose the periodic boundary conditions $S_{l+L}^\alpha \equiv S_l^\alpha$ $(\alpha = x, y, z)$. The spin operators obey the SU(2) algebra

$$\left[S_l^\alpha, S_{l'}^\beta \right] = i \delta_{l,l'} \epsilon^{\alpha\beta\gamma} S_l^\gamma, \quad \boldsymbol{S}_l^2 = \tfrac{3}{4}, \quad (2.1b)$$

with $\epsilon^{\alpha\beta\gamma}$ the fully antisymmetric Levi-Civita tensor where $\alpha, \beta, \gamma = x, y, z$ and $l, l' = 1, \ldots, L$. The exchange-anisotropy parameters Δ_y and Δ_z are non-negative numbers $(\Delta_y, \Delta_z \geqslant 0)$. The Hamiltonian thus depends on three dimensionless positive parameters, namely,

$$\mathcal{J} := \frac{J_2}{J_1} \geqslant 0, \quad \Delta_y \geqslant 0, \quad \Delta_z \geqslant 0. \quad (2.1c)$$

We restrict our discussion to the case of weak frustration

$$\mathcal{J} < \tfrac{1}{2} \quad (2.1d)$$

for which the nearest-neighbor exchange coupling J_1 is the dominant interaction and sets the dimension of energy. In other words, we are not concerned with other phases that can exist for $\mathcal{J} > \frac{1}{2}$, such as the UUDD (up-up-down-down) Neel-ordered phase that appears in the limit $\Delta_z \gg 1$, etc. When $\Delta_y = 0$, Hamiltonian (2.1a) is equivalent to the one recently studied by Jiang and Motrunich in Ref. [35]. Reference [36] also reports numerical simulations of the spin-$\frac{1}{2}$ XYZ Hamiltonian (2.1a).

We first discuss the symmetries of the model defined by Eq. (2.1). Hamiltonian H is invariant under the following transformations:

(i) π rotations about the x, y, and z axes in spin space

$$R_\pi^x : \left(S_l^x, S_l^y, S_l^z \right) \mapsto \left(S_l^x, -S_l^y, -S_l^z \right), \quad (2.2a)$$

$$R_\pi^y : \left(S_l^x, S_l^y, S_l^z \right) \mapsto \left(-S_l^x, S_l^y, -S_l^z \right), \quad (2.2b)$$

$$R_\pi^z : \left(S_l^x, S_l^y, S_l^z \right) \mapsto \left(-S_l^x, -S_l^y, S_l^z \right); \quad (2.2c)$$

(ii) translation by one lattice site

$$T : \left(S_l^x, S_l^y, S_l^z \right) \mapsto \left(S_{l+1}^x, S_{l+1}^y, S_{l+1}^z \right); \quad (2.2d)$$

(iii) inversion about the site $l = 0\,(\equiv L)$,

$$P : \left(S_l^x, S_l^y, S_l^z \right) \mapsto \left(S_{L-l}^x, S_{L-l}^y, S_{L-l}^z \right); \quad (2.2e)$$

(iv) time reversal

$$\Theta : \left(S_l^x, S_l^y, S_l^z\right) \mapsto \left(-S_l^x, -S_l^y, -S_l^z\right). \tag{2.2f}$$

We note that inversion about the center of a nearest-neighbor bond of the lattice is obtained by combining the site inversion P with the lattice translation T. Similarly, we note that $R_\pi^z = R_\pi^y R_\pi^x$. Equations (2.2a)–(2.2c) thus imply the existence of a global internal $\mathbb{Z}_2 \times \mathbb{Z}_2$ symmetry.

As we shall show in the following subsections, the ground-state phase diagram of the quantum spin-$\frac{1}{2}$ antiferromagnetic J_1-J_2 XYZ chain defined by Eq. (2.1) consists of the following four gapped phases: Neel$_x$, Neel$_y$, Neel$_z$, and valence-bond-solid (VBS or dimer) phases:

(1) Neel$_x$ phase. The symmetries R_π^y, R_π^z, T, Θ are spontaneously broken. The order parameter is

$$O_{\mathrm{N}_x} := \frac{1}{L}\sum_{l=1}^{L}(-1)^l \left\langle S_l^x \right\rangle, \tag{2.3a}$$

where we recall that L is the number of sites and $\langle A\rangle$ is the expectation value of the operator A in a ground state. The composition $T\,\Theta$ is a symmetry.

(2) Neel$_y$ phase. The symmetries R_π^z, R_π^x, T, Θ are spontaneously broken. The order parameter is

$$O_{\mathrm{N}_y} := \frac{1}{L}\sum_{l=1}^{L}(-1)^l \left\langle S_l^y \right\rangle. \tag{2.3b}$$

The composition $T\,\Theta$ is a symmetry.

(3) Neel$_z$ phase. The symmetries R_π^x, R_π^y, T, Θ are spontaneously broken. The order parameter is

$$O_{\mathrm{N}_z} := \frac{1}{L}\sum_{l=1}^{L}(-1)^l \left\langle S_l^z \right\rangle. \tag{2.3c}$$

The composition $T\,\Theta$ is a symmetry.

(4) VBS (dimer) phase. The symmetries P and T are spontaneously broken. We can take

$$O_{\mathrm{VBS}} := \frac{1}{L}\sum_{l=1}^{L}(-1)^l \left\langle S_l^x S_{l+1}^x + S_l^y S_{l+1}^y + S_l^z S_{l+1}^z \right\rangle \tag{2.3d}$$

as an order parameter of the VBS phase.

It is important to note that the $\mathbb{Z}_2$ symmetries R_π^α are broken in the Neel$_\beta$ phase provided $\alpha \neq \beta$, while the site-inversion symmetry P is broken in the VBS phase. Since the π rotation R_π^α and the inversion P are symmetries in the spin and real spaces, respectively, a direct continuous phase transition between a Neel phase and a VBS phase cannot be described by the Ginzburg-Landau theory. As we discuss below, the phase transitions between gapped ordered phases are continuous transitions described by a Gaussian theory with no less than a U(1) symmetry.

B. Phase diagram at $\Delta_y = 1$

We first discuss the case $\Delta_y = 1$ for which the Hamiltonian H describes the quantum spin-$\frac{1}{2}$ antiferromagnetic J_1-J_2 XXZ chain with an enhanced U(1) symmetry under continuous spin rotations about the z axis compared to the case when $\Delta_y \neq 1$. The quantum spin-$\frac{1}{2}$ antiferromagnetic J_1-J_2 XXZ chain has been studied in many publications [37–44]. Its ground-state phase diagram and low-energy effective theory are well understood; see e.g., Refs. [38,39]. We briefly review the low-energy effective theory, in order to fix notations and prepare for the full discussion of the ground-state phase diagram of the quantum spin-$\frac{1}{2}$ antiferromagnetic J_1-J_2 XYZ chain ($\Delta_y \neq 1$).

We introduce the Jordan-Wigner fermions c_l through the relations

$$S_l^z =: c_l^\dagger\, c_l - \frac{1}{2} \equiv n_l, \tag{2.4a}$$

$$S_l^+ \equiv S_l^x + iS_l^y =: c_l^\dagger\, \exp\left(i\pi \sum_{n<l} c_n^\dagger\, c_n\right), \tag{2.4b}$$

with which the Hamiltonian H at $\Delta_y = 1$ is rewritten as

$$\begin{aligned} H_{\mathrm{XXZ}} \equiv J_1 \sum_l \left[\frac{1}{2}(c_{l+1}^\dagger\, c_l + c_l^\dagger\, c_{l+1}) + \Delta_z\, n_l\, n_{l+1}\right] \\ + J_2 \sum_l [(c_{l+2}^\dagger c_l + c_l^\dagger c_{l+2}) n_{l+1} + \Delta_z n_l\, n_{l+2}]. \end{aligned} \tag{2.4c}$$

When both Δ_z and $\mathcal{J} \equiv J_2/J_1$ are zero, the Jordan-Wigner fermions are noninteracting and their energy band is half-filled. We introduce left- and right-moving fermions $\psi_L(x)$ and $\psi_R(x)$, which describe low-energy excitations near the two Fermi points at momentum $k = \pm\pi/2\mathfrak{a}$:

$$c_l \approx \sqrt{\mathfrak{a}}[e^{+i\pi x/(2\mathfrak{a})}\,\psi_L(x) + e^{-i\pi x/(2\mathfrak{a})}\,\psi_R(x)], \tag{2.5a}$$

where $x = l\,\mathfrak{a}$ with $\mathfrak{a}$ the lattice spacing. We take the continuum limit to approximate Hamiltonian H_{XXZ} by the integral $\int dx\, \mathcal{H}_{\mathrm{XXZ}}$ over the Hamiltonian density $\mathcal{H}_{\mathrm{XXZ}}$, where

$$\begin{aligned} \mathcal{H}_{\mathrm{XXZ}} = {} & iv(\psi_L^\dagger\, \partial_x \psi_L - \psi_R^\dagger\, \partial_x \psi_R) \\ & + g_+(:\psi_L^\dagger\, \psi_L: + :\psi_R^\dagger\, \psi_R:)^2 \\ & + g_-(:\psi_L^\dagger\, \psi_L: - :\psi_R^\dagger\, \psi_R:)^2 \\ & + g_{\mathrm{u}}(:\psi_L^\dagger\, \psi_L^\dagger:: \psi_R\, \psi_R: + :\psi_R^\dagger\, \psi_R^\dagger:: \psi_L\, \psi_L:). \end{aligned} \tag{2.5b}$$

Here, v is the velocity ($v > 0$), the coupling constants $g_\pm$ and g_{u} are matrix elements of forward and umklapp scatterings, and the normal-ordered operators are defined using point splitting, i.e., $:\mathcal{O}_A(x)\,\mathcal{O}_B(x):$ is the leading term from the Laurent expansion in powers of $\mathfrak{a}$ of $\mathcal{O}_A(x)\,\mathcal{O}_B(x+\mathfrak{a}) - \langle \mathcal{O}_A(x)\,\mathcal{O}_B(x+\mathfrak{a})\rangle$, where $\mathcal{O}_A$ and $\mathcal{O}_B$ are ψ_{M} or $\psi_{\mathrm{M}}^\dagger$ with $\mathrm{M} = \mathrm{L}, \mathrm{R}$.

Next, we bosonize the fermion fields using the formulas

$$\psi_{\mathrm{L}}(x) = \frac{e^{-i\varphi_{\mathrm{L}}(x)}}{\sqrt{2\pi\,\mathsf{a}}}, \quad \psi_{\mathrm{R}}(x) = \frac{e^{+i\varphi_{\mathrm{R}}(x)}}{\sqrt{2\pi\,\mathsf{a}}}, \tag{2.6a}$$

where a is a short-distance cutoff of the order of the lattice spacing $\mathfrak{a}$ and the chiral boson fields $\varphi_{\mathrm{M}}(x)$ with $\mathrm{M} = \mathrm{L}, \mathrm{R}$ satisfying the equal-time commutation relations

$$[\varphi_{\mathrm{R}}(x), \varphi_{\mathrm{R}}(y)] = -[\varphi_{\mathrm{L}}(x), \varphi_{\mathrm{L}}(y)] = i\pi\ \mathrm{sgn}(x-y), \tag{2.6b}$$

$$[\varphi_{\mathrm{R}}(x), \varphi_{\mathrm{L}}(y)] = i\pi. \tag{2.6c}$$

The Hamiltonian density, when expressed in terms of this pair of bosonic chiral fields, takes the form

$$\mathcal{H}_{\mathrm{XXZ}} = \frac{\tilde{g}_+}{8\pi}\left[\partial_x(\varphi_{\mathrm{L}}+\varphi_{\mathrm{R}})\right]^2 + \frac{\tilde{g}_-}{8\pi}\left[\partial_x(\varphi_{\mathrm{L}}-\varphi_{\mathrm{R}})\right]^2 + \tilde{g}_{\mathrm{u}}\cos[2(\varphi_{\mathrm{L}}+\varphi_{\mathrm{R}})]. \tag{2.6d}$$

Here, the parameters $\tilde{g}_\pm$ and $\tilde{g}_{\mathrm{u}}$ are given by

$$\tilde{g}_+ = \mathfrak{a} J_1\left[1+\frac{4}{\pi}(\Delta_z+\mathcal{J})\right], \tag{2.7a}$$

$$\tilde{g}_- = \mathfrak{a} J_1\left(1-\frac{4}{\pi}\mathcal{J}\right), \tag{2.7b}$$

$$\tilde{g}_{\mathrm{u}} = \frac{\mathfrak{a} J_1}{2\pi^2\mathsf{a}^2}[\Delta_z - \mathcal{J}(2+\Delta_z)], \tag{2.7c}$$

in the weak-coupling limit

$$0 \leqslant \Delta_z \ll 1, \quad 0 \leqslant \mathcal{J} \ll 1/2. \tag{2.7d}$$

However, the chiral representation (2.6d) of $\mathcal{H}_{\mathrm{XXZ}}$ holds beyond the perturbative regime (2.7d).

Instead of the chiral representation (2.6d) of $\mathcal{H}_{\mathrm{XXZ}}$, we shall use the sine-Gordon representation

$$\mathcal{H}_{\mathrm{XXZ}} = \frac{v}{2}\left[\frac{1}{\eta}(\partial_x\theta)^2 + \eta(\partial_x\phi)^2 + \lambda_\phi\cos(\sqrt{8\pi}\,\phi)\right], \tag{2.8a}$$

$$\frac{v}{2\eta} := \tilde{g}_-, \quad 2v\eta := \tilde{g}_+, \quad \frac{v\lambda_\phi}{2} := \tilde{g}_{\mathrm{u}}. \tag{2.8b}$$

The sine-Gordon Hamiltonian density $\mathcal{H}_{\mathrm{XXZ}}$ is invariant under any constant shift of θ. In other words, $\mathcal{H}_{\mathrm{XXZ}}$ is invariant under the global U(1) transformation

$$\theta \mapsto \theta + \text{constant}\ (\mathrm{mod}\ \sqrt{2\pi}), \quad \phi \mapsto \phi. \tag{2.8c}$$

The freedom in shifting θ by an arbitrary constant originates from the U(1) symmetry of the quantum spin-$\frac{1}{2}$ antiferromagnetic J_1-J_2 XXZ Hamiltonian, whereby the compactification radius $\sqrt{2\pi}$ stems from the relation (2.11) between the quantum spin-$\frac{1}{2}$ degrees of freedom on the lattice and the quantum fields ϕ and θ. The advantage of the sine-Gordon representation (2.8a) of $\mathcal{H}_{\mathrm{XXZ}}$ is that the parameter η has a simple interpretation. It controls the exponents of algebraic correlation functions when the cosine interaction is irrelevant. Here, we have adopted the conventions from Ref. [45] (see also references therein). The nonchiral bosonic fields ϕ and θ are dual to each other and defined by

$$\phi(x) := \frac{1}{\sqrt{2\pi}}[\varphi_{\mathrm{L}}(x)+\varphi_{\mathrm{R}}(x)], \tag{2.8d}$$

$$\theta(x) := \frac{1}{\sqrt{8\pi}}[\varphi_{\mathrm{L}}(x)-\varphi_{\mathrm{R}}(x)]. \tag{2.8e}$$

They inherit the commutation relation

$$[\phi(x),\theta(y)] = \mathrm{i}\Theta(y-x), \tag{2.8f}$$

where $\Theta(x)$ is the Heaviside function taking the value $\frac{1}{2}$ at the origin. We note that the dimensionful coupling constant $\lambda_\phi = 2\tilde{g}_{\mathrm{u}}/v$ is a function of Δ_z and $\mathcal{J}$. In the weak-coupling limit (2.7d), it is seen that λ_ϕ changes its sign from positive to negative as $\mathcal{J}$ is increased holding Δ_z fixed.

When the coupling λ_ϕ of the sine-Gordon interaction in the effective Hamiltonian density (2.8a) flows to zero in the low-energy limit, the ground state is a critical phase, the Tomonaga-Luttinger liquid (TLL) phase, described by the Gaussian Hamiltonian

$$H_\eta := \frac{v}{2}\int dx\left[\frac{1}{\eta}(\partial_x\theta)^2 + \eta(\partial_x\phi)^2\right]. \tag{2.9}$$

The TLL phase realizes a $c=1$ conformal field theory in $(1+1)$-dimensional space-time. It is invariant under the global U(1) transformation (2.8c). The Gaussian Hamiltonian (2.9) inherits this U(1) symmetry from that of the sine-Gordon Hamiltonian density (2.8a). Moreover, the Gaussian Hamiltonian (2.9) is also invariant under the global U(1) transformation

$$\phi \mapsto \phi + \text{constant}\ (\mathrm{mod}\ \sqrt{2\pi}), \quad \theta \mapsto \theta. \tag{2.10}$$

Therefore, the Gaussian Hamiltonian (2.9) has the $\mathrm{U}(1)_\theta \times \mathrm{U}(1)_\phi$ symmetry or, equivalently, the $\mathrm{U}(1)^{\mathrm{L}} \times \mathrm{U}(1)_{\mathrm{R}}$ symmetry. This global U(1)×U(1) symmetry is enhanced to a global SU(2) symmetry when $\Delta_y = \Delta_z = 1$ that originates from the SU(2) symmetry of the quantum spin-$\frac{1}{2}$ antiferromagnetic J_1-J_2 XXX Hamiltonian. At the SU(2) symmetric point $\Delta_y = \Delta_z = 1$, $\eta = 1$ must necessarily hold in the effective Hamiltonian (2.9). Conversely, if $\eta = 1$ holds in the effective theory, then $\mathcal{H}_{\eta=1}$ supports a global SU(2) symmetry, as we now explain.

The spin operators are related to the bosonic fields by

$$S^z_l \approx \frac{\mathfrak{a}}{\sqrt{2\pi}}\partial_x\phi(x) + a_1(-1)^l\sin(\sqrt{2\pi}\phi(x)), \tag{2.11a}$$

$$S^+_l \approx e^{+i\sqrt{2\pi}\theta(x)}\left[a_2(-1)^l + a_3\sin(\sqrt{2\pi}\phi(x))\right], \tag{2.11b}$$

where a_1, a_2, and a_3 are real numbers that are functions of $\mathcal{J}$ and Δ_z. From Eq. (2.11b) the S^x_l and S^y_l operators are written as

$$S^x_l = a_2(-1)^l\cos(\sqrt{2\pi}\,\theta(x)) + ia_3\sin(\sqrt{2\pi}\,\theta(x))\sin(\sqrt{2\pi}\,\phi(x)), \tag{2.12a}$$

$$S^y_l = a_2(-1)^l\sin(\sqrt{2\pi}\,\theta(x)) - ia_3\cos(\sqrt{2\pi}\,\theta(x))\sin(\sqrt{2\pi}\,\phi(x)). \tag{2.12b}$$

Here, the commutator $[\phi(x),\theta(x)] = i/2$ was used.

Motivated by the four order parameters (2.3a)–(2.3d) that were defined on the lattice, we define in the field theory the following four fields whose nonvanishing ground-state expectation value signals long-range order. From Eqs. (2.11a), (2.12a), and (2.12b), the triplet of fields whose nonvanishing ground-state expectation value signals Neel order are

$$N_x(x) := \cos(\sqrt{2\pi}\,\theta(x)), \tag{2.13a}$$

$$N_y(x) := \sin(\sqrt{2\pi}\,\theta(x)), \tag{2.13b}$$

$$N_z(x) := \sin(\sqrt{2\pi}\,\phi(x)). \tag{2.13c}$$

The field whose nonvanishing ground-state expectation value signals VBS (dimer) long-range order is [45]

$$D(x) := \cos(\sqrt{2\pi}\,\phi(x)). \tag{2.13d}$$

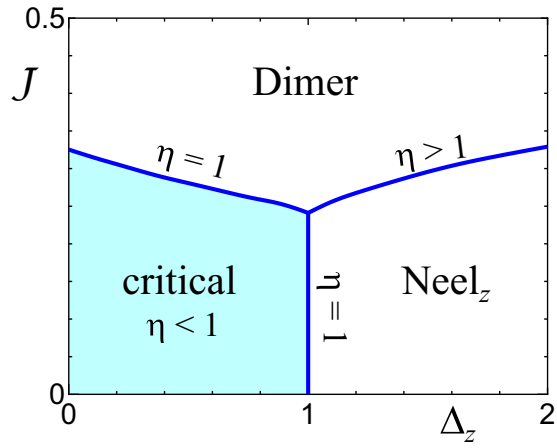

FIG. 1. Ground-state phase diagram of the quantum spin-$\frac{1}{2}$ antiferromagnetic J_1-J_2 XXZ Hamiltonian (2.4c) with the Ising exchange anisotropy Δ_z and the exchange ratio $\mathcal{J} = J_2/J_1$. The phase boundaries are taken from Ref. [38]. When $0 \leqslant \Delta_z < 1$ and $0 \leqslant \mathcal{J} < \mathcal{J}_c(\Delta_z)$, the system is in the critical phase with in-plane spin-correlation exponent $\eta < 1$ ($\eta = 1$ on the boundary of the critical phase). The umklapp coupling vanishes along the phase boundary with $\eta > 1$ separating the gapped dimer (VBS) and Neel$_z$ phases that break different $\mathbb{Z}_2$ symmetries.

The π rotations R^x_π, R^y_π, and R^z_π in spin space, the lattice translation T, the site inversion P, and the (antiunitary) time reversal Θ act on the bosonic fields as

$$R^x_\pi : (\phi, \theta) \mapsto (-\phi, -\theta), \tag{2.14a}$$

$$R^y_\pi : (\phi, \theta) \mapsto (-\phi, \sqrt{\pi/2} - \theta), \tag{2.14b}$$

$$R^z_\pi : (\phi, \theta) \mapsto (\phi, \theta + \sqrt{\pi/2}\,), \tag{2.14c}$$

$$T : (\phi, \theta) \mapsto (\phi + \sqrt{\pi/2}, \theta + \sqrt{\pi/2}\,), \tag{2.14d}$$

$$P : (\phi, \theta) \mapsto (-\phi + \sqrt{\pi/2}, \theta), \tag{2.14e}$$

$$\Theta : (\phi, \theta) \mapsto (-\phi, \theta + \sqrt{\pi/2}), \tag{2.14f}$$

respectively. The U(1) spin rotation symmetry about the z axis of the quantum spin-$\frac{1}{2}$ antiferromagnetic J_1-J_2 XXZ chain is generated by the infinitesimal transformation

$$(\phi, \theta) \mapsto (\phi, \theta + \delta\theta). \tag{2.15}$$

Figure 1 is a schematic picture of the ground-state phase diagram of the quantum spin-$\frac{1}{2}$ antiferromagnetic J_1-J_2 XXZ chain obtained by Haldane. The phase diagram supports a critical phase (extended over a finite region of parameter space) and two gapped phases. These long-range ordered phases are separated by a phase boundary that realizes a line of quantum critical points, each of which realizes a $c = 1$ conformal field theory with U(1) symmetry.

The critical phase defined by

$$0 \leqslant \Delta_z < 1, \quad 0 \leqslant \mathcal{J} < \mathcal{J}_c(\Delta_z) \tag{2.16}$$

is governed by the Gaussian Hamiltonian density $\mathcal{H}_\eta$ defined by Eq. (2.9) with $\eta < 1$. The parameter η takes the value $\eta = \frac{1}{2}$ at the free-fermion point $\mathcal{J} = \Delta_z = 0$ and continuously increases until $\eta = 1$, the value of which defines the phase boundaries to the gapped phases. The cosine term $\lambda_\phi \cos(\sqrt{8\pi}\,\phi)$ in the effective theory (2.8) has scaling dimension $2/\eta > 2$. It is thus an irrelevant perturbation to the Gaussian Hamiltonian (2.9). This critical phase is characterized by quasi-long-range order for all correlation functions of local operators. In particular, the two-point functions $\langle N_x(x)\, N_x(0)\rangle$ and $\langle N_y(x)\, N_y(0)\rangle$ show the slowest decay proportional to $|x|^{-\eta}$, whereas $\langle N_z(x)\, N_z(0)\rangle$ and $\langle D(x)\, D(0)\rangle$ decay like $|x|^{-1/\eta}$. The isotropy in the decay of the correlation functions $\langle N_x(x)\, N_x(0)\rangle$ and $\langle N_y(x)\, N_y(0)\rangle$ is a consequence of the global U(1) symmetry (2.15) that the Gaussian Hamiltonian (2.9) enjoys. At $\eta = 1$, all four two-point functions decay like $|x|^{-1}$. The isotropy in the decay of the correlation functions $\langle N_x(x)\, N_x(0)\rangle$, $\langle N_y(x)\, N_y(0)\rangle$, $\langle N_z(x)\, N_z(0)\rangle$ is a consequence of the hidden (nonmanifest) global SU(2) symmetry of $\mathcal{H}_\eta$ when $\eta = 1$. It follows that the critical points on the upper edge of the critical phase (2.16) shown in Fig. 1 have a global SU(2) symmetry.

Outside the critical phase (2.16), the cosine term $\lambda_\phi \cos(\sqrt{8\pi}\,\phi)$ is relevant and opens an energy gap. The resulting ground state is either the Neel$_z$ phase or the dimer phase, depending on the sign of the coupling constant λ_ϕ. If $\lambda_\phi < 0$, then the cosine term pins the ϕ field at $\phi = 0$ or $\sqrt{\pi/2}$ (mod $\sqrt{2\pi}$), and the dual field θ is disordered. This leads to $D = +1$ or -1 (if we ignore quantum fluctuations for simplicity), and $N_x = N_y = N_z = 0$; the ground state is in the dimer phase. If $\lambda_\phi > 0$, then the cosine term pins the ϕ field at $\phi = \sqrt{\pi/8}$ or $3\sqrt{\pi/8}$ (mod $\sqrt{2\pi}$), and the dual field θ is disordered. This leads to $N_z = +1$ or -1 (if we ignore quantum fluctuations for simplicity), and $D = N_x = N_y = 0$; the ground state is in the Neel$_z$ phase.

The phase transition between the dimer phase and the Neel$_z$ phase for $\Delta_z > 1$ is determined by the condition $\lambda_\phi = 0$; see Fig. 1. The critical theory at the phase transition is the $c = 1$ Gaussian Hamiltonian (2.9) with $\eta > 1$ [39]. At any dimer-Neel$_z$ critical point, the two-point functions $\langle N_z(x)\, N_z(0)\rangle$ and $\langle D(x)\, D(0)\rangle$ show the slowest algebraic decay $\sim|x|^{-1/\eta}$, whereas $\langle N_x(x)\, N_x(0)\rangle$ and $\langle N_y(x)\, N_y(0)\rangle$ decay like $\sim|x|^{-\eta}$.

Along the SU(2) invariant line $\Delta_z = 1$ the phase transition from the critical Tomonaga-Luttinger liquid phase to the dimer phase is known to occur at [37,42]

$$\mathcal{J} = \mathcal{J}_c^\star \equiv \mathcal{J}_c(\Delta_z = 1) = 0.2411\ldots. \tag{2.17}$$

We now examine the effects of breaking the U(1) symmetry (2.8c) with small $|\Delta_y - 1| > 0$. Following the steps of the Jordan-Wigner transformation and bosonization, we find that the deviation of Δ_y from unity yields the perturbation

$$\begin{aligned}(1 - \Delta_y)\big(S^x_l\, S^x_{l+1} - S^y_l\, S^y_{l+1}\big) &= \frac{1 - \Delta_y}{2}(S^+_l\, S^+_{l+1} + \text{H.c.}) \\ &\approx a_2^2(\Delta_y - 1)\cos(\sqrt{8\pi}\,\theta),\end{aligned} \tag{2.18}$$

which should be added to the effective theory (2.8). The operator $\cos(\sqrt{8\pi}\,\theta)$ is invariant under the transformations (2.14) and has the scaling dimension 2η. It is thus a relevant perturbation to the Gaussian Hamiltonian (2.9) with $\eta < 1$ in

the critical phase

$$0 \leqslant \Delta_z < 1, \quad 0 \leqslant \mathcal{J} < \mathcal{J}_c(\Delta_z), \quad \Delta_y = 1. \tag{2.19}$$

As such, the potential $(\Delta_y - 1)\cos(\sqrt{8\pi}\,\theta)$ pins the θ field at $\theta = 0$ or $\sqrt{\pi/2}$ (mod $\sqrt{2\pi}$) for $\Delta_y < 1$ and at $\theta = \sqrt{\pi/8}$ or $3\sqrt{\pi/8}$ (mod $\sqrt{2\pi}$) for $\Delta_y > 1$. This means that the critical phase (2.19) is located exactly on the boundary between the Neel$_x$ phase at $\Delta_y < 1$ and the Neel$_y$ phase at $\Delta_y > 1$. On the other hand, the $\cos(\sqrt{8\pi}\,\theta)$ operator is an irrelevant perturbation in both the dimer phase and the Neel$_z$ phase where the dual ϕ field is pinned by the $\cos(\sqrt{8\pi}\,\phi)$ perturbation. More importantly, the $\cos(\sqrt{8\pi}\,\theta)$ perturbation is an irrelevant perturbation to the Gaussian Hamiltonian (2.9) with $\eta > 1$ on the phase boundary between the Neel$_z$ and the dimer phases. Hence, the Neel$_z$-dimer phase boundary is a two-dimensional surface of $c = 1$ Gaussian criticality that extends out of the plane $\Delta_y = 1$.

It turns out that the criticality on the phase boundary between the dimer and Neel$_x$ phases or between the dimer and Neel$_y$ phases for $\Delta_y \neq 1$ is also described by the Gaussian Hamiltonian (2.9). On the upper edge of the critical phase (2.19), whose low-energy theory is the Gaussian model (2.9) with $\eta = 1$, both $\cos(\sqrt{8\pi}\,\phi)$ and $\cos(\sqrt{8\pi}\,\theta)$ are marginal operators with scaling dimension 2. The competition between these two dual operators is known [46] to yield a line of $c = 1$ fixed points, whose basin of attraction forms a critical plane of the Neel$_x$-dimer and Neel$_y$-dimer phase boundaries. We will discuss the criticality between gapped phases in more detail below.

C. Global phase diagram

We deduce the global phase diagram and criticality of the quantum spin-$\frac{1}{2}$ antiferromagnetic J_1-J_2 XYZ chain (2.1) from the analysis of the effective sine-Gordon Hamiltonian density (2.8) perturbed by (2.18). This prediction is validated numerically in Sec. II D. Parameter space for this phase diagram is the three-dimensional slab

$$\Delta_y \geqslant 0, \quad \Delta_z \geqslant 0, \quad 0 \leqslant \mathcal{J} \leqslant 1/2 \tag{2.20}$$

of $\mathbb{R}^3$. The global phase diagram for the ground states of Hamiltonian (2.1) is symmetric:

(1) about the plane defined by $\Delta_y = \Delta_z$ in the three-dimensional parameter space (2.20);

(2) under cyclic permutations of the indices x, y, and z entering either the anisotropies Δ_x, Δ_y, and Δ_z, where we have fixed $\Delta_x \equiv 1$, or the Neel phases Neel$_x$, Neel$_y$, and Neel$_z$.

We define $\mathcal{J}_c(\Delta_y, \Delta_z)$ to be the critical value of $\mathcal{J} \equiv J_2/J_1$ above which the ground state is in the dimer phase. By symmetry,

$$\mathcal{J}_c(\Delta_y, \Delta_z) = \mathcal{J}_c(\Delta_z, \Delta_y). \tag{2.21}$$

The phase diagram on the $\Delta_z = 1$ plane in the parameter space (2.20) follows from the phase diagram on the $\Delta_y = 1$ plane in the parameter space (2.20) that we derived in Sec. II B by interchanging the Neel$_y$ and Neel$_z$ phases. The phase diagram on the $\Delta_z = 1$ plane has thus three phases:

(i) the $c = 1$ critical phase with quasi-long-range order of the easy-plane Neel correlations (N_x, N_z) for

$$0 \leqslant \mathcal{J} < \mathcal{J}_c(\Delta_y, 1), \quad 0 \leqslant \Delta_y \leqslant 1; \tag{2.22a}$$

(ii) the Neel$_y$ phase for

$$0 \leqslant \mathcal{J} < \mathcal{J}_c(\Delta_y, 1), \quad \Delta_y > 1; \tag{2.22b}$$

(iii) the dimer phase for

$$\mathcal{J} > \mathcal{J}_c(\Delta_y, 1). \tag{2.22c}$$

The phase boundary between the Neel$_y$ phase and the dimer phase is a line of $c = 1$ critical points with $\eta > 1$.

Similarly, the phase diagram on the plane defined by $\Delta_y = \Delta_z$ is also obtained from the phase diagram on the $\Delta_y = 1$ plane by replacing Δ_z with $1/\Delta_z$ in the horizontal axis in Fig. 1 and by exchanging the Neel$_z$ and Neel$_x$ phases. By this logic, there are three phases on the $\Delta_z = \Delta_y$ plane:

(i) the $c = 1$ critical phase with quasi-long-range order of the easy-plane Neel correlations (N_z, N_y) for

$$0 \leqslant \mathcal{J} < \mathcal{J}_c(\Delta_z, \Delta_z), \quad \Delta_z > 1; \tag{2.23a}$$

(ii) the Neel$_x$ phase for

$$0 \leqslant \mathcal{J} < \mathcal{J}_c(\Delta_z, \Delta_z) \quad 0 \leqslant \Delta_z < 1; \tag{2.23b}$$

(iii) the dimer phase for

$$\mathcal{J} > \mathcal{J}_c(\Delta_z, \Delta_z). \tag{2.23c}$$

Examples (2.22) and (2.23) illustrate that, whereas the condition

$$\mathcal{J} > \mathcal{J}_c(\Delta_y, \Delta_z) \tag{2.24}$$

always selects the dimer phase in the parameter space (2.20), the condition

$$\mathcal{J} < \mathcal{J}_c(\Delta_y, \Delta_z) \tag{2.25}$$

selects either one of the three Neel phases or the critical manifold separating them. Which one of the Neel phases is selected depends on which of the anisotropies Δ_y or Δ_z is the largest:

(a) the Neel$_x$ phase is selected when

$$\Delta_y < 1, \quad \Delta_z < 1; \tag{2.26a}$$

(b) the Neel$_y$ phase is selected when

$$\Delta_y > 1, \quad \Delta_y > \Delta_z; \tag{2.26b}$$

(c) the Neel$_z$ phase is selected when

$$\Delta_z > 1, \quad \Delta_z > \Delta_y. \tag{2.26c}$$

The phase boundaries between these three Neel phases are the $c = 1$ critical phases located on the $\Delta_y = 1$ plane, $\Delta_z = 1$ plane, or $\Delta_y = \Delta_z$ plane, which cross at the SU(2) symmetric line $\Delta_y = \Delta_z = 1$. A schematic picture of the phase diagram in the three-dimensional parameter space $(\Delta_y, \Delta_z, \mathcal{J})$ is shown in Fig. 2.

The criticality at the Neel-dimer and Neel-Neel phase transitions can be studied perturbatively near a special point along the SU(2) symmetric segment [recall Eq. (2.17)]

$$\Delta_y = \Delta_z = 1, \quad 0 \leqslant \mathcal{J} \leqslant \mathcal{J}_c^\star, \quad \mathcal{J}_c^\star := \mathcal{J}_c(1, 1). \tag{2.27}$$

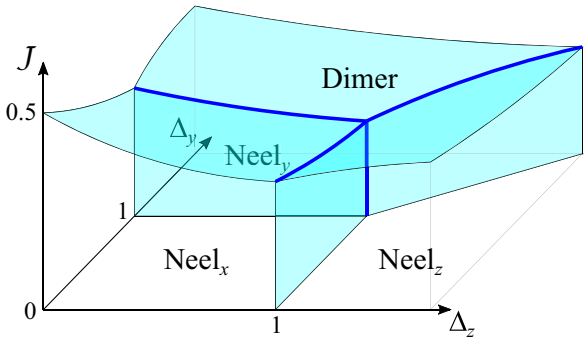

FIG. 2. Qualitative phase diagram of the quantum spin-$\frac{1}{2}$ antiferromagnetic J_1-J_2 XYZ model in the three-dimensional parameter space $(\Delta_z, \Delta_y, \mathcal{J})$. The three Neel phases and the dimer phase are separated by six planes of phase boundaries, each of which realizes Gaussian criticality with U(1)×U(1) symmetry. These six planes join at the four solid blue lines, along which the fixed-point theory is the Gaussian model with SU(2) symmetry. The dimer phase exists for $\mathcal{J} > \mathcal{J}_c(\Delta_y, \Delta_z)$. The three Neel$_\alpha$ phases with $\alpha = x, y, z$ are located below the phase boundaries of the Gaussian criticality $\mathcal{J} < \mathcal{J}_c(\Delta_y, \Delta_z)$. The pair of Neel$_\alpha$ and Neel$_\beta$ phases with $\alpha < \beta = x, y, z$ are separated by the phase boundary at $\Delta_\alpha = \Delta_\beta$ of the Gaussian criticality ($\Delta_x \equiv 1$). We have omitted other phases (such as the UUDD Ising ordered phase) that can exist for $\mathcal{J} > \frac{1}{2}$.

At the special point

$$\Delta_y = \Delta_z = 1, \quad \mathcal{J} = \mathcal{J}_c^\star, \tag{2.28}$$

the low-energy theory is the Gaussian Hamiltonian density with $\eta = 1$, i.e.,

$$\mathcal{H}_0 \equiv \tfrac{1}{2}[(\partial_x\theta)^2 + (\partial_x\phi)^2], \tag{2.29}$$

where we have set $v = 1$ for simplicity. Away from this special point, the effective Hamiltonian density is perturbed by local operators that are invariant under the symmetry transformations (2.14). Among all such local operators, the less irrelevant ones at the special point (2.28) in parameter space (2.20) are the three marginal operators

$$\cos(\sqrt{8\pi}\,\phi), \quad \cos(\sqrt{8\pi}\,\theta), \quad (\partial_x\phi)^2 - (\partial_x\theta)^2, \tag{2.30}$$

for they all share the scaling dimension 2 when $\eta = 1$. They are related to the chiral generators of the su(2)$_1$ affine Lie algebra by

$$J_{\rm L}^\pm := \frac{1}{\mathfrak{a}}\, e^{\pm i\sqrt{2}\phi_{\rm L}}, \quad J_{\rm L}^z := \frac{1}{\sqrt{2}}\,\partial_x\phi_{\rm L}, \tag{2.31a}$$

$$J_{\rm R}^\pm := \frac{1}{\mathfrak{a}}\, e^{\mp i\sqrt{2}\phi_{\rm R}}, \quad J_{\rm R}^z := \frac{1}{\sqrt{2}}\,\partial_x\phi_{\rm R}, \tag{2.31b}$$

where we have introduced yet a second pair of left- and right-moving chiral bosonic fields, namely,

$$\phi_{\rm L}(x) := \sqrt{\pi}[\phi(x) + \theta(x)], \quad \phi_{\rm R}(x) := \sqrt{\pi}[\phi(x) - \theta(x)]. \tag{2.31c}$$

Here, we chose the normalization convention for the left- and right-moving currents $J_{\rm M}^\pm$ with ${\rm M} = {\rm L}, {\rm R}$ such that $\langle J_{\rm M}^+(x)\, J_{\rm M}^-(0)\rangle = -1/x^2$ for the SU(2) symmetric Gaussian Hamiltonian (2.29). The microscopic origin of the components $J_{\rm M}^\pm(x)$ and $J_{\rm M}^z(x)$ is the following. The nonoscillating components of the spin operators S_l^z and S_l^+ in Eqs. (2.11a) and (2.11b) are equal to $\mathfrak{a}/\sqrt{\pi}$ times $J_{\rm L}^z + J_{\rm R}^z$ and $J_{\rm L}^+ + J_{\rm R}^+$, respectively, at $\eta = 1$. If we define the linear combinations

$$J_{\rm M}^x := \frac{J_{\rm M}^+ + J_{\rm M}^-}{2}, \quad J_{\rm M}^y := \frac{J_{\rm M}^+ - J_{\rm M}^-}{2i}, \quad {\rm M} = {\rm L}, {\rm R} \tag{2.32a}$$

we may then define the current-current interaction density [47]

$$\begin{aligned}\mathcal{H}_{JJ} &:= \lambda_x J_{\rm L}^x J_{\rm R}^x + \lambda_y J_{\rm L}^y J_{\rm R}^y + \lambda_z J_{\rm L}^z J_{\rm R}^z \\ &= -\frac{1}{\mathfrak{a}^2}(\lambda_x - \lambda_y)\cos(\sqrt{8\pi}\,\theta) \\ &\quad - \frac{1}{\mathfrak{a}^2}(\lambda_x + \lambda_y)\cos(\sqrt{8\pi}\,\phi) \\ &\quad - \frac{\pi\lambda_z}{2}[(\partial_x\theta)^2 - (\partial_x\phi)^2],\end{aligned} \tag{2.32b}$$

where the real-valued couplings λ_x, λ_y, and λ_z are dimensionless.

The perturbed Hamiltonian density $\mathcal{H}_0 + \mathcal{H}_{JJ}$ should be compared with the perturbed Hamiltonian density $\mathcal{H}_{\rm XXZ} + \frac{A}{\mathfrak{a}^2}(\Delta_y - 1)\cos(\sqrt{8\pi}\,\theta)$, where A is a nonuniversal positive number of order one, by demanding that

$$\mathcal{H}_0 + \mathcal{H}_{JJ} = \mathcal{H}_{\rm XXZ} + \frac{A}{\mathfrak{a}^2}\,(\Delta_y - 1)\cos(\sqrt{8\pi}\,\theta). \tag{2.33}$$

By matching the couplings of $\cos(\sqrt{8\pi}\,\theta)$ on both sides of this equation and using the symmetry under cyclic permutations of the indices x, y, and z with $\Delta_x \equiv 1$, we infer that

$$\lambda_x - \lambda_y = A\,(1 - \Delta_y), \tag{2.34a}$$

$$\lambda_y - \lambda_z = A\,(\Delta_y - \Delta_z), \tag{2.34b}$$

$$\lambda_z - \lambda_x = A\,(\Delta_z - 1). \tag{2.34c}$$

Furthermore, by matching the coefficients of $(\partial_x\theta)^2$ and $(\partial_x\phi)^2$ on both sides of this equation, we deduce that

$$\eta = \sqrt{\frac{1 + \pi\lambda_z}{1 - \pi\lambda_z}}. \tag{2.35a}$$

In particular,

$$\eta \approx 1 + \pi\lambda_z \tag{2.35b}$$

when $|\lambda_z| \ll 1$. Finally, remembering that the scaling dimensions of $\cos(\sqrt{8\pi}\,\theta)$ and $\cos(\sqrt{8\pi}\,\phi)$ in the Gaussian theory (2.9) are

$$2\eta \approx 2 + 2\pi\,\lambda_z, \quad |\lambda_z| \ll 1 \tag{2.36a}$$

and

$$\frac{2}{\eta} \approx 2 - 2\pi\,\lambda_z, \quad |\lambda_z| \ll 1 \tag{2.36b}$$

respectively, we deduce from the renormalization-group (RG) equation $dO/d\ell = (2 - d_O)\,O$ in (1+1)-dimensional spacetime, where $d\ell = d\ln\mathfrak{a}$ and O is an operator whose exact

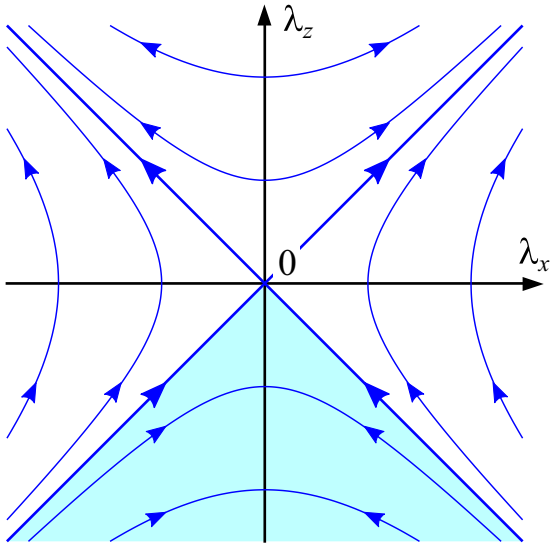

FIG. 3. Renormalization-group flow diagram of Eq. (2.38) on the $\lambda_x = \lambda_y$ plane. The shaded region corresponds to the critical phase in Fig. 1.

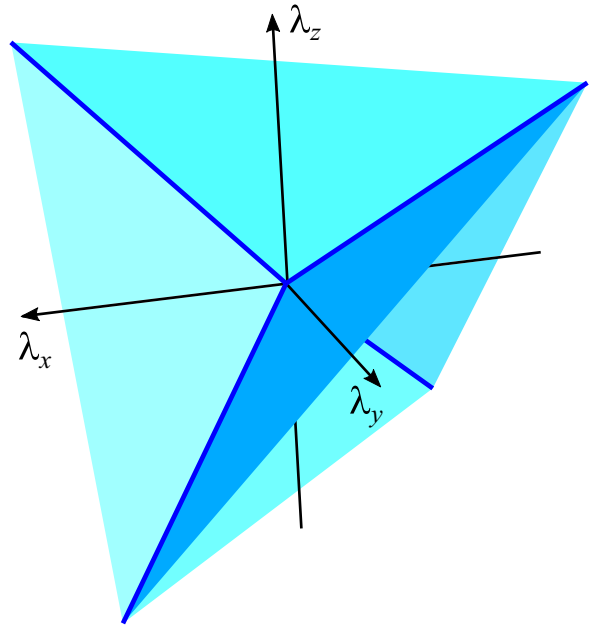

FIG. 4. Six critical planes separating four gapped phases in the three-dimensional parameter space $(\lambda_x, \lambda_y, \lambda_z)$.

scaling dimension is d_O, the one-loop RG flows

$$\frac{d(\lambda_x - \lambda_y)}{d\ell} = -2\pi\lambda_z(\lambda_x - \lambda_y), \tag{2.37a}$$

$$\frac{d(\lambda_x + \lambda_y)}{d\ell} = +2\pi\lambda_z(\lambda_x + \lambda_y), \tag{2.37b}$$

for $|\lambda_x - \lambda_y|, |\lambda_x + \lambda_y|, |\lambda_z| \ll 1$. With the help of cyclic permutations of the indices x, y, and z, we thus obtain the one-loop RG equations

$$\frac{d\lambda_x}{d\ell} = 2\pi\,\lambda_y\,\lambda_z, \quad \frac{d\lambda_y}{d\ell} = 2\pi\,\lambda_z\,\lambda_x, \quad \frac{d\lambda_z}{d\ell} = 2\pi\,\lambda_x\,\lambda_y, \tag{2.38}$$

for the couplings λ_x, λ_y, λ_z of the current-current interaction density (2.32b) at the Gaussian fixed point (2.29).

The coupled flow equations (2.38) have three lines of fixed points: (i) $\lambda_x = \lambda_y = 0$, (ii) $\lambda_y = \lambda_z = 0$, and (iii) $\lambda_z = \lambda_x = 0$, where the fixed-point Hamiltonian is given by Eq. (2.9). Let us consider RG flows on the $\lambda_x = \lambda_y$ plane, for example; see Fig. 3. On this plane the RG flows in the region defined by $\lambda_z \leqslant -|\lambda_x|$ end up on λ_z axis with $\lambda_z < 0$. The boundary of this critical region is the diagonal $\lambda_x = \pm\lambda_z$ for $\lambda_z < 0$ flowing to the origin $\lambda_x = \lambda_y = \lambda_z = 0$. The RG flows on the $\lambda_x = -\lambda_y$ plane are the reverse of those on the $\lambda_x = \lambda_y$ plane, and the critical region on the $\lambda_x = -\lambda_y$ plane is given by $\lambda_z > |\lambda_x|$. Similar RG flows can be obtained for the $\lambda_y = \pm\lambda_z$ plane and the $\lambda_z = \pm\lambda_x$ plane. From these considerations we find that the three-dimensional parameter space $(\lambda_x, \lambda_y, \lambda_z)$ has six critical planes on which the low-energy theory is the Gaussian Hamiltonian (2.9); see Fig. 4. The six critical planes form the boundaries of four gapped phases corresponding to the Neel$_x$, Neel$_y$, Neel$_z$, and dimer phases.

We note that the critical phase at $\Delta_z < 1$ in Fig. 1 corresponds to the critical region $\lambda_z < -|\lambda_x|$ on the $\lambda_x = \lambda_y$ plane. The phase transition between the Neel$_z$ and dimer phases at $\Delta_z > 1$ corresponds to the positive half of the λ_z axis. We thus deduce that

$$\lambda_z = b\,(\mathcal{J} - \mathcal{J}_c^\star) + c\left(\Delta_z - \frac{1+\Delta_y}{2}\right), \tag{2.39a}$$

where $\Delta_y = 1$ in Fig. 1 and b and c are positive constants. By cyclic permutations of the indices x, y, and z with $\Delta_x \equiv 1$, we obtain

$$\lambda_x = b\,(\mathcal{J} - \mathcal{J}_c^\star) + c\left(1 - \frac{\Delta_y + \Delta_z}{2}\right), \tag{2.39b}$$

$$\lambda_y = b\,(\mathcal{J} - \mathcal{J}_c^\star) + c\left(\Delta_y - \frac{\Delta_z + 1}{2}\right). \tag{2.39c}$$

Consistency with Eq. (2.34) demands here that $c = 2A/3$.

This perturbative RG analysis is justified for $|\Delta_y - 1|, |\Delta_z - 1|, |\mathcal{J} - \mathcal{J}_c^\star| \ll 1$. However, we expect that the global picture of the phase diagram and the $c = 1$ Gaussian criticality (2.9) at the phase boundaries should generally be valid beyond this perturbative regime. Furthermore, the phase transitions between a Neel phase and a dimer phase are the Gaussian criticality (2.9) with $\eta > 1$ while the phase transitions between Neel phases are that with $\eta < 1$. At a Neel$_\alpha$-dimer transition with $\alpha = x, y, z$ defined by the condition

$$\mathcal{J} = \mathcal{J}_c \tag{2.40a}$$

(the dependence of $\mathcal{J}_c$ on Δ_y and Δ_z is implicit), the dependencies on the length L of the chain for the Neel and dimer order parameters are power laws with the same scaling exponent,

$$\langle N_\alpha \rangle \sim \langle D \rangle \sim L^{-1/(2\eta)}. \tag{2.40b}$$

Moreover, in the thermodynamic limit $L \to \infty$, their dependencies on $\mathcal{J} - \mathcal{J}_c$ are the power laws

$$\langle N_\alpha \rangle \sim (\mathcal{J}_c - \mathcal{J})^{1/[4(\eta-1)]}\, \Theta(\mathcal{J}_c - \mathcal{J}), \quad (2.40c)$$

$$\langle D \rangle \sim (\mathcal{J} - \mathcal{J}_c)^{1/[4(\eta-1)]}\, \Theta(\mathcal{J} - \mathcal{J}_c), \quad (2.40d)$$

where $\Theta(x)$ is the Heaviside function, respectively. Similarly, at the Neel$_\alpha$-Neel$_\beta$ transition with $\alpha < \beta = x, y, z$ defined by the condition

$$\Delta_\alpha = \Delta_\beta, \quad (2.41a)$$

the Neel$_\alpha$ and the Neel$_\beta$ order parameters also vanish as power laws as a function of the length L of the chain with the same scaling exponent

$$\langle N_\alpha \rangle \sim \langle N_\beta \rangle \sim L^{-\eta/2}. \quad (2.41b)$$

Hereto, in the thermodynamic limit $L \to \infty$, their dependencies on $\Delta_\alpha - \Delta_\beta$ are the power laws

$$\langle N_\alpha \rangle \sim (\Delta_\alpha - \Delta_\beta)^{\eta/[4(1-\eta)]}\, \Theta(\Delta_\alpha - \Delta_\beta), \quad (2.41c)$$

$$\langle N_\beta \rangle \sim (\Delta_\beta - \Delta_\alpha)^{\eta/[4(1-\eta)]}\, \Theta(\Delta_\beta - \Delta_\alpha), \quad (2.41d)$$

respectively. Equations (2.40) and (2.41) express the duality

$$\mathcal{J} - \mathcal{J}_c,\ \eta \longleftrightarrow \Delta_\beta - \Delta_\alpha,\ 1/\eta \quad (2.42)$$

at the level of the scaling variables and the scaling exponents between the Neel-dimer and the Neel$_\alpha$-Neel$_\beta$ transitions. Thereto, the Neel$_\alpha$-Neel$_\beta$ transition is an example of a phase transition beyond the Landau-Ginzburg paradigm, as it separates two gapped phases breaking spontaneously distinct $\mathbb{Z}_2$ sectors of the $\mathbb{Z}_2 \times \mathbb{Z}_2$ symmetry in spin space of the quantum spin-$\frac{1}{2}$ antiferromagnetic J_1-J_2 XYZ Hamiltonian (2.1).

Finally, we stress that the critical theory has an emergent U(1)×U(1) symmetry that is enhanced relative to the discrete symmetries ($\mathbb{Z}_2 \times \mathbb{Z}_2$ in spin space, $\mathbb{Z} \times \mathbb{Z}_2$ of 1D lattice, and $\mathbb{Z}_2$ in time) of the quantum spin-$\frac{1}{2}$ antiferromagnetic J_1-J_2 XYZ Hamiltonian (2.1). We have performed numerical studies to confirm this conjecture.

D. Numerical results

We are going to study the phase diagram of the quantum spin-$\frac{1}{2}$ antiferromagnetic J_1-J_2 XYZ Hamiltonian (2.1a) numerically using two complementary methods, namely, exact diagonalization and DMRG. We will confirm numerically that, by varying the dimensionless coupling $\mathcal{J} \equiv J_2/J_1$ while holding Δ_y and Δ_z fixed to suitable values, Hamiltonian (2.1a) undergoes a quantum phase transition between a Neel$_\alpha$ with $\alpha = x, y, z$ phase and a dimer phase within the $c = 1$ Gaussian universality class in $(1 + 1)$-dimensional space-time. To this end, we shall study exclusively the phase transition between the Neel$_z$ and dimer phases. Indeed, the relations between the phase transitions separating the Neel$_\alpha$ phase with $\alpha = x, y$ from the dimer phase and the phase transition between the Neel$_z$ and dimer phases were given in Sec. II C. As a typical example, we focus on the two-dimensional cut

$$\Delta_z = 2.0, \quad 0 \leqslant \Delta_y < \Delta_z, \quad 0 \leqslant \mathcal{J} < 0.5 \quad (2.43)$$

from the three-dimensional parameter space (2.20) in which the Neel$_z$ to dimer quantum transition is expected to take place.

We first analyze the eigenenergy spectrum of the quantum spin-$\frac{1}{2}$ antiferromagnetic J_1-J_2 XYZ Hamiltonian (2.1a) for a chain hosting L spins obeying periodic boundary conditions. We assume that L is an even integer. Eigenstates with ascending eigenenergies are denoted $\Psi_0(L)$, $\Psi_1(L)$, $\Psi_2(L)$, etc. Their eigenenergies are denoted $E_0(L)$, $E_1(L)$, $E_2(L)$, etc. The finite-size excitation gap above the ground state is defined by

$$\Delta E_0(L) := E_1(L) - E_0(L). \quad (2.44)$$

The finite-size excitation gap above the first excited state is defined by

$$\Delta E_1(L) := E_2(L) - E_1(L), \quad (2.45)$$

and so on. The dependence of $\Delta E_0(L)$ on $\mathcal{J}$ should be qualitatively different depending on whether the system is at or away from a critical point, as we explain below. On the one hand, deep either in the Neel$_z$ or dimer phases, $\Delta E_0(L)$ is expected to decay exponentially fast to zero with increasing L, while $\Delta E_1(L)$ remains nonvanishing in the thermodynamic limit $L \to \infty$. Hence, the finite-size ground and first-excited states become degenerate while remaining linearly independent in the thermodynamic limit $L \to \infty$, for which a continuum of excitations is separated from the twofold-degenerate ground states by a gap. On the other hand, at a putative continuous quantum critical point separating the Neel$_z$ phase from the dimer phase, the finite-size gap $\Delta E_0(L)$ between ground and first-excited states is expected to decay algebraically to zero with increasing L, with a level crossing of the first-excited state $\Psi_1(L)$ whose inversion quantum number differs between the Neel$_z$ side and the dimer side. According to this scenario, we may identify a putative continuous quantum critical point separating the Neel$_z$ phase from the dimer phase by a cusp singularity in the dependence of $\Delta E_0(L)$ on $\mathcal{J}$ for fixed Δ_y, Δ_z, and L. Indeed, this scenario was verified for the quantum spin-$\frac{1}{2}$ antiferromagnetic J_1-J_2 XXZ chain in Ref. [38].

For several values of Δ_y, we have computed the finite-size excitation gap (2.44) along the one-dimensional cuts

$$\Delta_z = 2.0, \quad 0 \leqslant \mathcal{J} < 0.5 \quad (2.46)$$

of the two-dimensional cut (2.43) for L increasing from $L = 8$ to 20 using the exact diagonalization (Lanczos) method. Our results for the one-dimensional cut with $\Delta_y = 0.5$ are presented in Fig. 5(a), by plotting the dependence of $L\,\Delta E_0(L)$ on $\mathcal{J}$. The cusp singularity of the dependence on $\mathcal{J}$ of the finite-size excitation gap (2.44) signals the anticipated level crossing of the first-excited states $\Psi_1(L)$ on the Neel$_z$ side crossing energetically with $\Psi_1(L)$ on the dimer side of the critical point $\mathcal{J}_c$. On both sides of the cusp, the scaled finite-size gap $L\,\Delta E_0(L)$ decays with L, suggesting the rapid decay (faster than $1/L$) of $\Delta E_0(L)$ in the gapped phases. We also find that $L\,\Delta E_0(L)$ at the cusp is almost independent of L, indicating the critical scaling of the gap $\Delta E_0(L) \sim 1/L$. These numerical results support our conjecture that the quantum spin-$\frac{1}{2}$ antiferromagnetic J_1-J_2 XYZ Hamiltonian (2.1a) with Δ_y suitably chosen undergoes a continuous quantum phase transition between the Neel$_z$ and dimer phases with a dynamical scaling exponent $z = 1$ upon varying $\mathcal{J}$.

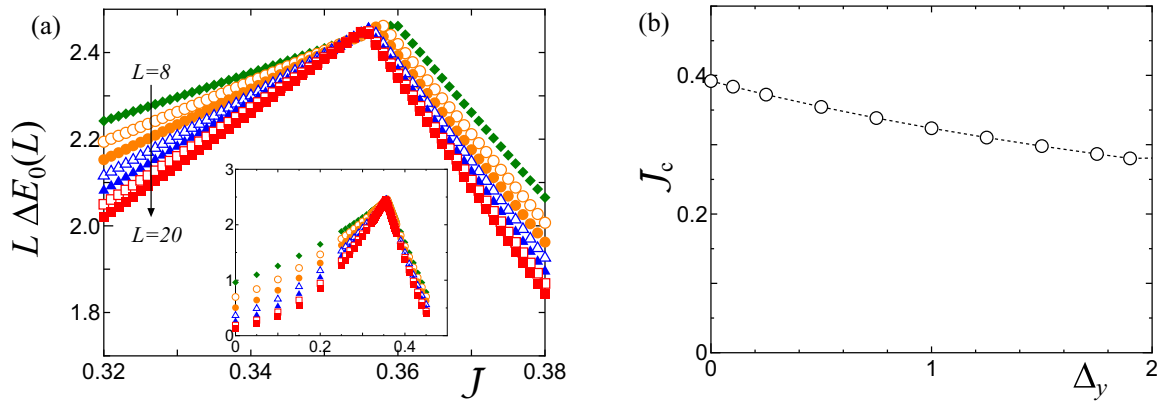

FIG. 5. (a) Dependence on $\mathcal{J} \equiv J_2/J_1$ of the scaled finite-size gap $L\,\Delta E_0(L)$ with $\Delta E_0(L)$ defined in Eq. (2.44) for $\Delta_y = 0.5$, $\Delta_z = 2.0$, and $L = 8$ to 20. The position of the cusp defines $\mathcal{J}_c(L)$. The inset shows the data for the range $0 \leqslant \mathcal{J} < 1/2$, while the main panel limits the range of data to the vicinity of the cusp singularity. (b) Critical coupling $\mathcal{J}_c = \lim_{L\to\infty} \mathcal{J}_c(L)$ at which a continuous quantum phase transition separates the Neel$_z$ from the dimer phase for $\Delta_z = 2.0$ as a function of $0 \leqslant \Delta_y < 2.0$.

We have extrapolated the critical value $\mathcal{J}_c(L)$ determined above by fitting the data to a second-order polynomial of $1/L$ (see Appendix). The extrapolated value of the critical coupling $\mathcal{J}_c$ is shown in Fig. 5(b) as a function of Δ_y. With increasing Δ_y, $\mathcal{J}_c$ runs from $\mathcal{J}_c = 0.3918(9)$ at $\Delta_y = 0$ toward $\mathcal{J}_c = 0.276$ at $\Delta_y = \Delta_z = 2.0$, the latter was obtained in Ref. [38].

Second, we determine the central charge at the continuous quantum critical point separating the Neel$_z$ and dimer phases. For this purpose, we analyze the entanglement entropy $\mathcal{S}(l)$ between the left l-site block and the right $(L-l)$-site block in the ground state of the quantum spin-$\frac{1}{2}$ antiferromagnetic J_1-J_2 XYZ Hamiltonian (2.1a) when open boundary conditions are imposed. It is known that the entanglement entropy at criticality in $(1+1)$-dimensional space-time scales with l as [48–52]

$$\mathcal{S}(l) = \frac{c}{6}\ln[f(x_l)] + \alpha_{\rm osc}\,E_{\rm osc}(l) + \mathcal{S}_0, \tag{2.47a}$$

where c is the central charge, the function

$$f(x_l) := \frac{L+1}{\pi}\,\sin\left(\frac{\pi\,x_l}{L+1}\right), \quad x_l := l + \frac{1}{2} \tag{2.47b}$$

is the effective size of the left l-site block, $\alpha_{\rm osc}$ is a constant, the oscillating component of the local bond-energy expectation value $E_{\rm osc}(l)$ is defined in Eq. (A3), and $\mathcal{S}_0$ is a constant. We can therefore estimate the central charge c from the slope of the uniform contribution

$$\mathcal{S}_{\rm uni}(l) := \mathcal{S}(l) - \alpha_{\rm osc}\,E_{\rm osc}(l) \tag{2.47c}$$

to the entanglement entropy $\mathcal{S}(l)$ plotted as a function of $\ln[f(l+\frac{1}{2})]$.

Using the DMRG method, we have computed the entanglement entropy $\mathcal{S}(l)$ and the oscillating part $E_{\rm osc}(l)$ of the local bond-energy expectation value for the quantum spin-$\frac{1}{2}$ antiferromagnetic J_1-J_2 XYZ Hamiltonian (2.1a) for an open chain hosting up to $L = 192$ spins at all the continuous quantum critical points from Fig. 5(b) separating the Neel$_z$ phase from the dimer phase. Results for $\Delta_y = 0.5$ are summarized in Fig. 6. For all the critical values of $\mathcal{J}_c$ obtained in Fig. 5(b), we find the central charge c obtained for $L = 192$ to be in the range $0.993 < c < 1.000$, in agreement with the analytical arguments supporting the claim that all Neel$_{\alpha=x,y,z}$-dimer quantum critical points realize a $c = 1$ Gaussian conformal field theory (CFT) in $(1+1)$-dimensional space-time.

Finally, we estimate the critical exponent η at the transition. To this end, we have calculated the expectation value of the local dimer-order operator

$$O_{\rm VBS}(L) := \left\langle S^x_{\frac{L}{2}}\,S^x_{\frac{L}{2}+1} + S^y_{\frac{L}{2}}\,S^y_{\frac{L}{2}+1} + S^z_{\frac{L}{2}}\,S^z_{\frac{L}{2}+1}\right\rangle_L - \left\langle S^x_{\frac{L}{2}-1}\,S^x_{\frac{L}{2}} + S^y_{\frac{L}{2}-1}\,S^y_{\frac{L}{2}} + S^z_{\frac{L}{2}-1}\,S^z_{\frac{L}{2}}\right\rangle_L \tag{2.48}$$

at the center of an open chain of length L (L is chosen a multiple of four). Here, $\langle A\rangle_L$ denotes the ground-state expectation value of the operator A for an open chain of length L. At a continuous quantum critical point, $O_{\rm VBS}(L)$ is expected to behave as

$$O_{\rm VBS}(L) \sim L^{-\frac{1}{2\eta}}. \tag{2.49}$$

Figure 7(a) presents our DMRG data of $O_{\rm VBS}(L)$ for $\Delta_z = 2.0$, $\Delta_y = 0.5$, and $\mathcal{J} = \mathcal{J}_c$. They show the expected scaling behavior (2.49). The estimates of η obtained from the fitting outlined in Appendix are shown in Fig. 7(b). It is found that, as anticipated, $\eta > 1$ for $0 \leqslant \Delta_y < \Delta_z$ and η approaches unity as Δ_y approaches Δ_z, $\eta - 1 \propto \sqrt{2-\Delta_y}$.

E. Revisiting the Neel$_z$-VBS transition

Having obtained the numerical evidence that the dimer-Neel$_\alpha$ phase boundaries [i.e., the critical values $\mathcal{J}_c(\Delta_y, \Delta_z)$] realize a $c = 1$ conformal field theory in (1+1)-dimensional space-time for a wide range in the two-dimensional parameter space (Δ_y, Δ_z), we return to the dimer-Neel$_z$ phase transition at $\Delta_z > 1$ for $|\Delta_y - 1| \ll 1$. Our aim is to give a complementary description of this transition.

As a warmup exercise, we consider first the bosonized theory (2.8). Because $\eta > 1$ in the Hamiltonian density (2.8a), the operator $\cos(\sqrt{8\pi}\,\theta)$ is irrelevant and thus plays only a minor role close to the Neel$_z$-dimer transition, a role that we shall ignore. By inspection of Eq. (2.13c) we deduce that the ϕ field is pinned at either $\phi = \sqrt{\pi/8}$ or $3\sqrt{\pi/8}$ (mod $\sqrt{2\pi}$) in the Neel$_z$ phase. These two values correspond to two

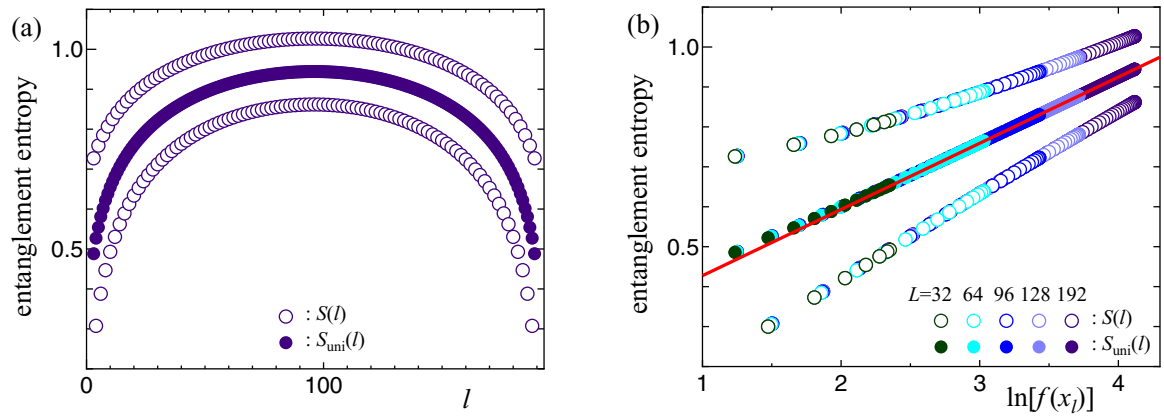

FIG. 6. Entanglement entropy $\mathcal{S}(l)$ (open circles) and its uniform part $\mathcal{S}_{\rm uni}(l)$ (filled circles) at the quantum critical point $\mathcal{J} = \mathcal{J}_{\rm c}$ for $\Delta_z = 2.0$ and $\Delta_y = 0.5$. (a) $\mathcal{S}(l)$ and $\mathcal{S}_{\rm uni}(l)$ for $L = 192$ are plotted as a function of l. Successive open circles are either above or below the curve defined by the filled circles. This effect originates from choosing open boundary conditions. (b) $\mathcal{S}(l)$ and $\mathcal{S}_{\rm uni}(l)$ for $L = 32, 64, 96, 128, 192$ are plotted as a function of $\ln[f(x_l)]$ with $x_l := l + \frac{1}{2}$.

degenerate Ising-ordered states in the Neel$_z$ phase. Suppose that the ground state is in the Neel$_z$ phase and that there is a domain wall between the two Ising-ordered states [e.g., $\phi = \sqrt{\pi/8}$ for $x < 0$ and $\phi = 3\sqrt{\pi/8}$ for $x > 0$ as shown in Fig. 8(a)]. At the domain wall the ϕ field displays a kink structure that crosses $\phi = 0$ or $\sqrt{\pi/2}$ (mod $\sqrt{2\pi}$), where the dimer order parameter (2.13d) takes a nonvanishing expectation value $D = \cos(\sqrt{2\pi}\phi) \neq 0$. Conversely, suppose that the ground state is in the dimer phase in which there is a domain wall between the two degenerate dimer-ordered states. By Eq. (2.13d), the ϕ field must then be pinned at either $\phi = 0$ or $\sqrt{\pi/2}$ (mod $\sqrt{2\pi}$). At the domain wall the ϕ field displays a kink structure that crosses $\phi = \sqrt{\pi/8}$ or $3\sqrt{\pi/8}$ (mod $\sqrt{2\pi}$) as shown in Fig. 8(b), where the Neel$_z$ order parameter (2.13c) takes a nonvanishing expectation value $N_z = \sin(\sqrt{2\pi}\phi) \neq 0$. Therefore, the center of a domain wall in the Neel$_z$ phase supports a local dimer order and, conversely, a domain wall in the dimer phase supports a local Neel$_z$ order.

We may draw a parallel to the scenario of deconfined quantum criticality in two spatial dimensions that separate easy-plane Neel order from dimer order. On the one hand, U(1) vortices in the Neel-ordered phase nucleate local dimer order. On the other hand, $\mathbb{Z}_4$ vortices in the dimer-ordered phase nucleate local easy-plane Neel order. The proliferation of these point defects in one of the ordered phases destroys this phase in favor of long-range order in the competing phase [7–9].

Let us return to the fermionic theory with the Hamiltonians (2.4c) and (2.5b). We first note that the local Neel$_z$ operator can be written in the fermion representation as

$$n_z(x) = \psi_{\rm L}^\dagger(x)\,\psi_{\rm R}(x) + \psi_{\rm R}^\dagger(x)\,\psi_{\rm L}(x) = \Psi^\dagger(x)\,\sigma_1\,\Psi(x), \tag{2.50a}$$

while the local dimer operator can be written as

$$d(x) = -i\psi_{\rm L}^\dagger(x)\,\psi_{\rm R}(x) + i\psi_{\rm R}^\dagger(x)\,\psi_{\rm L}(x) = \Psi^\dagger(x)\,\sigma_2\,\Psi(x), \tag{2.50b}$$

where σ_1, σ_2, and σ_3 are Pauli matrices, and

$$\Psi(x) \equiv \begin{pmatrix} \psi_{\rm L}(x) \\ \psi_{\rm R}(x) \end{pmatrix}. \tag{2.50c}$$

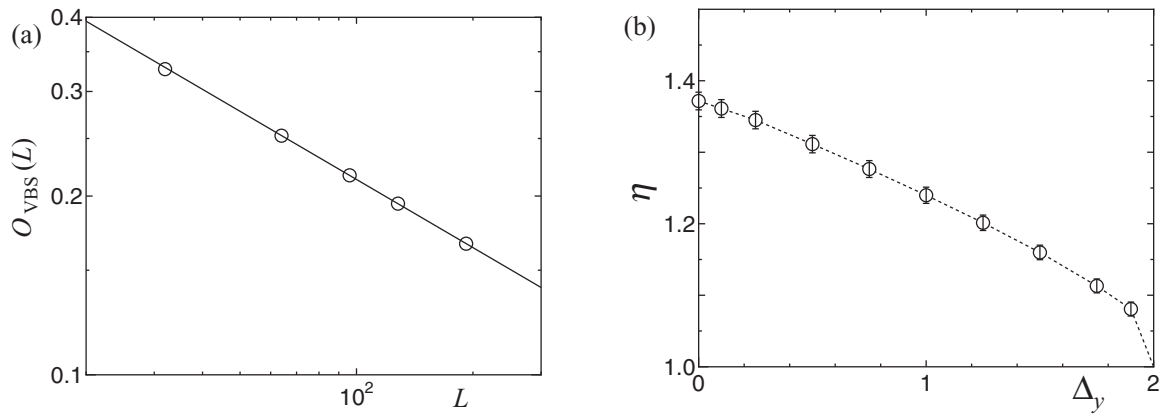

FIG. 7. (a) Log-log plot of the dependence of $O_{\rm VBS}(L)$ defined in Eq. (2.48) on L at the critical point $\mathcal{J} = \mathcal{J}_{\rm c}$ for $\Delta_z = 2.0$ and $\Delta_y = 0.5$. (b) Exponent η at the Neel$_z$-dimer transition for $\Delta_z = 2.0$ as a function of Δ_y.

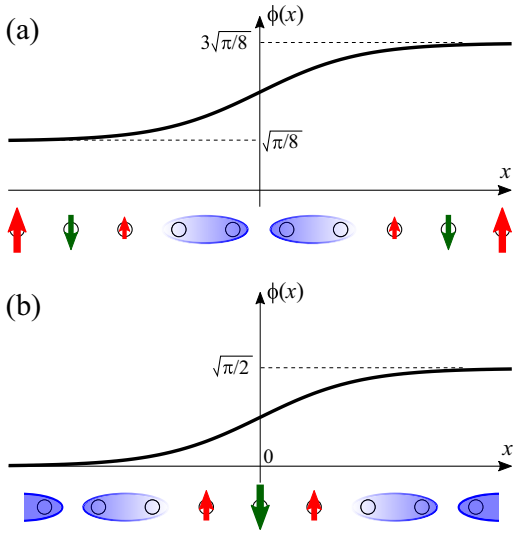

FIG. 8. Schematic picture of a domain wall in (a) the Neel$_z$ phase and (b) the VBS (dimer) phase.

Equation (2.50b) is obtained from the oscillating contributions in $S^+_l S^-_{l+1} + S^-_l S^+_{l+1} = c^\dagger_{l+1} c_l + c^\dagger_l c_{l+1}$ and $S^z_l S^z_{l+1} = n_l n_{l+1}$. Equations (2.50a) and (2.50b) encode the correspondence $(n_z, d) \leftrightarrow (\sigma_1, \sigma_2)$ between the local pair of order parameters (n_z, d) and the pair of Pauli matrices, i.e., two elements of a Clifford algebra.

Taking the two local order operators n_z and d as mean fields (or Hubbard-Stratonovich fields), we replace the XXZ Hamiltonian density (2.5b) with the mean field Dirac Hamiltonian density

$$\mathcal{H}_{\rm MF}(x) := iv(\Psi^\dagger \sigma_3 \partial_x \Psi)(x) - g_n\, n_z(x)\, (\Psi^\dagger \sigma_1\, \Psi)(x) - g_d\, d(x)\, (\Psi^\dagger\, \sigma_2\, \Psi)(x), \tag{2.51}$$

which is to be supplemented by the additive Hubbard-Stratonovich (HS) contributions

$$\mathcal{H}_{\rm HS}(x) := g_n\, n_z^2(x) + g_d\, d^2(x), \tag{2.52}$$

where the couplings g_n and g_d are related to the couplings $g_{\rm u}$ and $g_\pm$ entering the XXZ Hamiltonian density (2.5b). Integrating out the Hubbard-Stratonovich fields n_z and d reproduces $\mathcal{H}_{\rm XXZ}$ approximately. Therefore, $\mathcal{H}_{\rm MF}$ can be used as a starting point for the discussion of the Neel$_z$-dimer phase transition. It is important to point out that the two order parameters n_z and d are Dirac mass terms when they are constants in (1+1)-dimensional space-time.

Suppose that we are in the Neel$_z$ phase, in which there is a domain wall. We thus assume $n_z(x) = n_z^0 \tanh(x/\xi)$ and $d(x) = 0$, where ξ is a width of the domain wall. We then find that there is a zero mode localized at $x = 0$, which is an eigenstate of σ_2 [53]. This implies that the dimer order is locally generated at the center of a domain wall in the Neel$_z$ phase. Conversely, if we are in the dimer phase with a domain wall, where $d(x) = d_0 \tanh(x/\xi)$ and $n_z(x) = 0$. Again we obtain a zero mode localized at $x = 0$, which is an eigenstate of σ_1 [53]. This implies that the Neel$_z$ order is locally generated at the center of a domain wall in the dimer phase. These considerations run parallel to the discussion on domain walls in the bosonized theory.

Next, we consider deriving from $\mathcal{H}_{\rm MF}$ an effective theory for the Neel$_z$-dimer phase transition by integrating out the Dirac fermions $\psi_{\rm M}$ with ${\rm M} = {\rm L}, {\rm R}$. To this end, the two order-parameter fields n_z and d are regarded as elements of the vector field

$$\boldsymbol{n} := (d, n_z) \tag{2.53a}$$

on which we impose the nonlinear constraint

$$\boldsymbol{n}^2 = 1. \tag{2.53b}$$

A by-product of this nonlinear constraint is that it regularizes the domain walls supported by either one of the pair n_z and d in such a way that $\boldsymbol{n}$ points locally toward d when n_z vanishes and conversely. In this way, the zero modes from the previous paragraph are moved to a finite energy. Integration over the Dirac fermions in the partition function is now safe.

Expanding the Dirac-fermion determinant in a gradient expansion of the smooth fluctuations about a saddle point corresponding to a mean field solution $\boldsymbol{n} = \boldsymbol{n}_0$, we obtain, after analytical continuation of time t to imaginary time τ, the Euclidean effective action given by

$$S_0 = \frac{1}{2g} \int d\tau \int dx\, [(\partial_\tau \boldsymbol{n})^2 + (\partial_x \boldsymbol{n})^2]. \tag{2.54}$$

Here, we have set the velocity to be unity for simplicity. The stiffness g is a positive dimensionless coupling constant. The smooth unit vector field $\boldsymbol{n}$ may be parametrized by a smooth angle φ through

$$\boldsymbol{n} = (d, n) = (\cos\varphi, \sin\varphi), \tag{2.55}$$

in which case the action S_0 is now represented by the Gaussian action

$$S_0 = \frac{1}{2g} \int d\tau \int dx\, [(\partial_\tau \varphi)^2 + (\partial_x \varphi)^2]. \tag{2.56}$$

Very much as was the case with Eqs. (2.13c) and (2.13d), the long-range Neel$_z$ order corresponds to pinning φ to the values

$$\varphi = \frac{\pi}{2}, \frac{3\pi}{2} \pmod{2\pi}, \tag{2.57a}$$

while the long-range dimer order corresponds to pinning φ to the values

$$\varphi = 0, \pi \pmod{2\pi}. \tag{2.57b}$$

The four extrema (2.57a) and (2.57b) of $\cos\varphi$ and $\sin\varphi$ on the interval $0 \leqslant \varphi < 2\pi$ are the four local minima of $-\lambda_4 \cos(4\varphi)$ on the same interval with $\lambda_4 > 0$. We thus add to S_0 the potential $-\lambda_4 \cos(4\varphi)$ to stabilize the Neel$_z$ and dimer phases. Furthermore, we can introduce another potential $\lambda_\varphi \cos(2\varphi)$ that selects either the Neel$_z$ or dimer order depending on the sign of the coupling constant λ_φ. We note that the potential $-\lambda_4 \cos(4\varphi)$ reduces the symmetry from U(1) in S_0 to $\mathbb{Z}_4$, and the potential $\lambda_\varphi \cos(2\varphi)$ further reduces the symmetry to $\mathbb{Z}_2 \times \mathbb{Z}_2$.

Similarly to the classical XY model in two-dimensional space, the unit vector $\boldsymbol{n}$ need not be smooth as it may support point defects in the form of vortices in (1+1)-dimensional

space-time. The vorticities of such point defects are a topological attribute such as the charge one vortex at the origin given by

$$\varphi_{\rm vtx}(\tau, x) := \arctan\Big(\frac{x}{\tau}\Big), \tag{2.58}$$

say. It turns out, however, that the relevant vortices to the Neel$_z$-dimer transition are the charge ± 2 vortices, as we will explain below. The presence of such charge ± 2 vortices can be taken into account by adding to the Lagrangian density in Eq. (2.56) the cosine potential [46,54,55]

$$\mathcal{L}_{\rm vtx} := \lambda_\vartheta \cos(4\pi\vartheta), \tag{2.59}$$

where the coupling λ_ϑ is dimensionful. Here, the field ϑ is related to the field φ by the Cauchy-Riemann conditions

$$\partial_x\varphi = +ig\,\partial_\tau\vartheta, \quad \partial_\tau\varphi = -ig\,\partial_x\vartheta, \tag{2.60a}$$

once the measure for φ has been augmented to accommodate vortices. Alternatively, in the operator formalism, we must demand the equal-time commutation relation

$$[\varphi(x), \vartheta(y)] = i\Theta(y-x) \tag{2.60b}$$

with the convention $\Theta(0) \equiv \frac{1}{2}$ for the Heaviside function.

We have therefore deduced the effective Lagrangian density [56]

$$\begin{aligned}\mathcal{L}_{\mathbb{Z}_2\times\mathbb{Z}_2} := &-i\partial_x\vartheta\,\partial_\tau\varphi + \frac{g}{2}(\partial_x\vartheta)^2 + \frac{1}{2g}(\partial_x\varphi)^2 \\ &+ \lambda_\vartheta\,\cos(4\pi\vartheta) + \lambda_\varphi\,\cos(2\varphi) - \lambda_4\,\cos(4\varphi),\end{aligned} \tag{2.61}$$

where λ_ϑ, λ_φ, λ_4 are dimensionful coupling constants, and $\lambda_4 > 0$. The effective Lagrangian density $\mathcal{L}_{\mathbb{Z}_2\times\mathbb{Z}_2}$ is to be compared with the Hamiltonian H_0 perturbed by the current-current interaction H_{JJ} through the identifying (φ, ϑ) with $(\sqrt{2\pi}\phi, \theta/\sqrt{2\pi})$. As we have discussed in Sec. II C, the critical theory at the Neel$_z$-dimer phase transition is the Gaussian Hamiltonian (2.9) with the continuous parameter $\eta > 1$ and a U(1)×U(1) symmetry. At the Neel$_z$-dimer transition, the renormalized coupling constant λ_φ vanishes, while the interaction $\lambda_4\cos(4\varphi)$ is irrelevant and thus vanishes in the long-distance limit. The parameter η is related to $1/g$. In the Hamiltonian picture, the role of the dual potential $\lambda_\vartheta\cos(4\pi\vartheta)$ is to create a 4π kink in the φ field, as seen from the relation

$$e^{i4\pi\vartheta(y)}\varphi(x)e^{-i4\pi\vartheta(y)} = \varphi(x) + 4\pi\,\Theta(y-x). \tag{2.62}$$

It is important to realize that the shift of $\varphi(x)$ at $x = y$ is 2π, the period of the φ field. The potential $\cos(2\pi\vartheta)$ corresponding to charge one vortices would introduce a $\pm\pi$ shift and therefore is not allowed in the effective action. As we have seen in Sec. II B, the physical origin of the $\cos(4\pi\vartheta)$ potential, or the $\cos(\sqrt{8\pi}\theta)$ potential invariant under (2.14), is $S^+_l S^+_{l+1} + S^-_l S^-_{l+1}$. It is also interesting to point out the analogy to the case of $(2+1)$-dimensional space-time for which no monopoles with a charge less than four appear in the effective theory of deconfined quantum criticality [7–9], while no vortices with a vorticity less than two appear here.

III. DIRAC SEMIMETALLIC PHASE IN ($d > 1$)-DIMENSIONAL SPACE PERTURBED BY A CONTACT INTERACTION

When the dimensionality d of space is $d = 1$, we have shown in Sec. II that the quantum spin-$\frac{1}{2}$ antiferromagnetic J_1-J_2 XYZ chain supports a pair of gapped phases at zero temperature, each of which breaks spontaneously an Ising symmetry, that are separated by a continuous phase transition with an enlarged U(1)×U(1) continuous symmetry. One phase is an Ising Neel phase. The other phase is a valence-bond-solid (VBS or dimer) phase. The driving mechanism for this transition is the proliferation of a dual pair of domain walls. The duality means here that a domain wall in the Ising Neel ordered phase nucleates locally the Ising VBS order, while the converse also holds, i.e., a domain wall in the Ising VBS ordered phase nucleates locally the Ising Neel order. At the quantum critical point, both dual domain walls have proliferated extensively.

Inspired by Sec. II E, we are going to present a general framework to describe Neel-VBS quantum phase transition beyond Landau-Ginzburg theory and related phenomena by using a model of Dirac fermions in three-dimensional space ($d = 3$) with contact interactions. This is a generalization of the approach taken for $d = 2$ by Tanaka and Hu [10] and by Senthil and Fisher [11]. In their work, it was shown that the effective action for the Neel and VBS order parameter fields takes the form of a nonlinear sigma model (NLSM) with a topological term. In particular, for a quantum phase transition between an easy-plane Neel phase and a VBS phase, the O(4) nonlinear sigma model with a theta term is obtained as an effective theory and its connection to the noncompact CP^1 model was discussed [11].

Our model for $d = 3$ supports a pair of long-range ordered phases at vanishing temperature that break spontaneously the symmetries of the Hamiltonian, namely, Neel ordering that breaks the (internal) spin-$\frac{1}{2}$ SU(2) symmetry and VBS (dimer) ordering that breaks the translation and rotation symmetries of some underlying cubic lattice model. We propose the two possibilities that these phases are either separated by a continuous phase transition with an enlarged continuous symmetry or by a gapless spin-liquid phase that is extended in parameter space. Hereto, the driving mechanism for these two possibilities is the proliferation of a dual pair of topological defects.

We will first introduce a tight-binding model on the cubic lattice and a Dirac Hamiltonian in the continuum limit. The Neel and dimer order parameters are related to Dirac mass terms in the Dirac Hamiltonian. Integrating out the Dirac fermions gives a bosonic effective field theory for the order-parameter fields, which is a NLSM augmented by a Wess-Zumino term. The RG flow for this NLSM will be used to conjecture the fate of the semimetallic phase defined by the π-flux phase on the cubic lattice at half-filling, when perturbed by certain local quartic fermionic interactions preserving an O(3) × O(3) symmetry.

A. The π-flux phase in three-dimensional space and its instabilities

In this section, we show that the π-flux phase on the cubic lattice for spinless electrons accommodates an eight-dimensional representation of the Dirac Hamiltonian at the

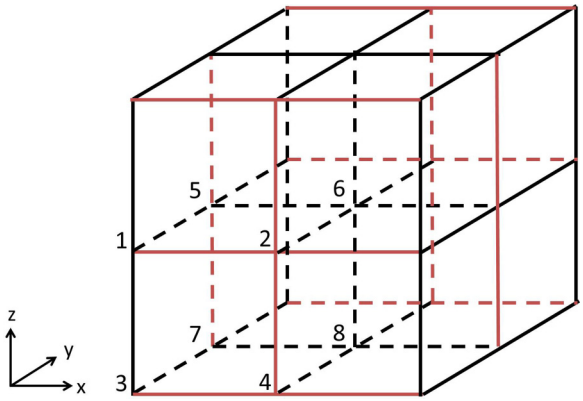

FIG. 9. We define the π-flux model on the three-dimensional cubic lattice by the following rules. Only nearest-neighbor hopping amplitudes are allowed. All nearest-neighbor hopping amplitudes have the magnitude $t/2 > 0$ and are real valued. The sign of the nearest-neighbor hopping amplitudes is $+1$ (-1) when the nearest-neighbor is colored in black (red).

corner (π, π, π) of the π-flux phase Brillouin zone. We show that there are four mass terms at the Dirac point that anticommute pairwise and are compatible with time-reversal symmetry and fermion-number conservation, three of which are compatible with chiral symmetry, one of which breaks the chiral symmetry. If time-reversal symmetry and fermion-number conservation are both broken, the corresponding 16-dimensional representation of the Bogoliubov–de Gennes Dirac Hamiltonian can be shown to accommodate two additional massive channels that, together with the four previous ones, anticommute pairwise [57]. Alternatively, we show below that the π-flux phase on the cubic lattice for spinful electrons also accommodates a 16-dimensional representation of the Dirac Hamiltonian with six mass terms at the Dirac point that anticommute pairwise and are compatible with fermion-number conservation. Three of those masses are associated to valence-bond (dimer) ordering, while the other three are associated to antiferromagnetic (Neel) order that breaks the SU(2) spin symmetry down to a U(1) subgroup.

We consider a cubic lattice with the lattice spacing $\mathfrak{a}/2$, which we partition into eight sublattices with a cubic repeated unit cell whose volume is $\mathfrak{a}^3$. This repeated unit cell contains eight nonequivalent sites, as is shown in Fig. 9. The site 3 of this repeated unit cell is assigned the coordinate $\boldsymbol{i} \in \mathbb{Z}^3$. To each $\boldsymbol{i}$, we assign the eight-component wave function

$$\Psi_{\boldsymbol{i}} \equiv (\psi_{i1}\, \psi_{i2}\, \psi_{i3}\, \psi_{i4}\, \psi_{i5}\, \psi_{i6}\, \psi_{i7}\, \psi_{i8})^{\mathsf{T}} \in \mathbb{C}^8. \tag{3.1}$$

The local Hilbert space $\mathbb{C}^8$ can be represented by the span of the 16 Hermitian matrices

$$X_{\mu_1\mu_2\mu_3} := \tau_{\mu_1} \otimes \upsilon_{\mu_2} \otimes \zeta_{\mu_3}, \quad \mu_1, \mu_2, \mu_3 = 0, 1, 2, 3 \tag{3.2a}$$

where τ_μ, υ_μ, and ζ_μ each denote a quadruplet of unit 2×2 matrix ($\mu = 0$) and Pauli matrices ($\mu = 1, 2, 3$) and the action of the Pauli matrices τ_3, υ_3, and ζ_3 on the wave function Ψ_i is defined by the following rules. The matrix

$$X_{300} = \tau_3 \otimes \upsilon_0 \otimes \zeta_0 \tag{3.2b}$$

has the eigenvalues $+1$ and -1 when Ψ_i is only nonvanishing on the face with the vertices (1,3,5,7) and (2,4,6,8) in the yz plane of the repeat unit cell, respectively. The matrix

$$X_{003} = \tau_0 \otimes \upsilon_0 \otimes \zeta_3 \tag{3.2c}$$

has the eigenvalues $+1$ and -1 when Ψ_i is only nonvanishing on the face with the vertices (1,2,3,4) and (5,6,7,8) in the zx plane of the repeat unit cell, respectively. The matrix

$$X_{030} = \tau_0 \otimes \upsilon_3 \otimes \zeta_0 \tag{3.2d}$$

has the eigenvalues $+1$ and -1 when Ψ_i is only nonvanishing on the face with the vertices (1,2,5,6) and (3,4,7,8) in the xy plane of the repeat unit cell, respectively.

We define a tight-binding model by the following rules. Only nearest-neighbor hopping amplitudes are allowed. All nearest-neighbor hopping amplitudes have the magnitude $t/2 > 0$ and are real valued. The sign of the nearest-neighbor hopping amplitudes is $+1$ (-1) when the nearest neighbor is colored in black (red) in Fig. 9.

Hopping along the positive x direction in Fig. 9 takes wave functions localized on the face (1,3,5,7) in Fig. 9 to wave functions localized on the face (2,4,6,8) and conversely. This process is encoded by the product

$$\Gamma_1 \equiv -X_{103} \tag{3.3a}$$

of the matrices

$$X_{100} = \tau_1 \otimes \upsilon_0 \otimes \zeta_0, \ -X_{003} = -\tau_0 \otimes \upsilon_0 \otimes \zeta_3, \tag{3.3b}$$

by inspection of Fig. 9. Hopping along the positive y direction in Fig. 9 takes wave functions localized on the face (1,2,3,4) in Fig. 9 to wave functions localized on the face (5,6,7,8) and conversely. This process is encoded by the product

$$\Gamma_2 \equiv +X_{001} \tag{3.4a}$$

of the matrices

$$X_{001} = \tau_0 \otimes \upsilon_0 \otimes \zeta_1, \ X_{000} = \tau_0 \otimes \upsilon_0 \otimes \zeta_0, \tag{3.4b}$$

by inspection of Fig. 9. Hopping along the positive z direction in Fig. 9 takes wave functions localized on the face (3,4,7,8) in Fig. 9 to wave functions localized on the face (1,2,5,6) and conversely. This process is encoded by the product

$$\Gamma_3 \equiv +X_{313} \tag{3.5a}$$

of the matrices

$$X_{010} = \tau_0 \otimes \upsilon_1 \otimes \zeta_0, \quad X_{303} = \tau_3 \otimes \upsilon_0 \otimes \zeta_3, \tag{3.5b}$$

by inspection of Fig. 9. If we choose units such that $\mathfrak{a} = t = 1$, the tight-binding Hamiltonian defined by Fig. 9 is thus represented by

$$\mathscr{H}_{\boldsymbol{k}}^{\text{kin}} := \cos k_x\, \Gamma_1 + \cos k_y\, \Gamma_2 + \cos k_z\, \Gamma_3 \tag{3.6a}$$

in the first Brillouin zone

$$-\frac{\pi}{2} \leqslant k_x \leqslant \frac{\pi}{2}, \quad -\frac{\pi}{2} \leqslant k_y \leqslant \frac{\pi}{2}, \quad -\frac{\pi}{2} \leqslant k_z \leqslant \frac{\pi}{2}, \tag{3.6b}$$

associated with the repeated unit cell of unit volume, where we have set $\mathfrak{a} = 1$.

The eigenvalues of $\mathscr{H}_{\boldsymbol{k}}^{\text{kin}}$ are fourfold degenerate and come in pairs of opposite signs

$$\varepsilon_{\boldsymbol{k}} = \pm\sqrt{\cos^2 k_x + \cos^2 k_y + \cos^2 k_z}. \tag{3.7}$$

The upper fourfold-degenerate band touches the lower fourfold-degenerate band at the eight corners

$$\boldsymbol{k}_{\text{D}}^{(\pm,\pm,\pm)} := \left(\pm\tfrac{1}{2}, \pm\tfrac{1}{2}, \pm\tfrac{1}{2}\right) \tag{3.8}$$

of the Brillouin zone. All those corners are equivalent modulo a reciprocal wave vector. We may then choose the Dirac point to be

$$\boldsymbol{k}_{\text{D}} := \left(\tfrac{1}{2}, \tfrac{1}{2}, \tfrac{1}{2}\right) \tag{3.9}$$

without loss of generality. Expanding to linear order around the Dirac point $\mathscr{H}_{\boldsymbol{k}}^{\text{kin}}$ delivers an eight-dimensional representation of the massless Dirac Hamiltonian in three-dimensional space. This representation is twice as large as the four-dimensional representation of the original Dirac Hamiltonian. This is an example of fermion doubling.

So far, all hopping amplitudes from Fig. 9 have the same magnitude $t/2$. This assumption can be relaxed by demanding that two consecutive nearest-neighbor bonds along the directions x, y, and z within the repeat unit cell are changed by the substitutions

$$\frac{t}{2} \mapsto \frac{t}{2} \mp \frac{d_x}{2}, \quad \frac{t}{2} \mapsto \frac{t}{2} \pm \frac{d_y}{2}, \quad \frac{t}{2} \mapsto \frac{t}{2} \pm \frac{d_z}{2}, \tag{3.10}$$

with $d_x, d_y, d_z \in \mathbb{R}$, respectively. With this substitution,

$$\mathscr{H}_{\boldsymbol{k}}^{\text{kin}} \mapsto \mathscr{H}_{\boldsymbol{k}}^{\text{kin}} + \mathscr{V}_{\boldsymbol{k}}^{\text{VB}} \tag{3.11a}$$

with

$$\mathscr{V}_{\boldsymbol{k}}^{\text{VB}} = d_x \sin k_x \, \Gamma_4 + d_y \sin k_y \, \Gamma_5 + d_z \sin k_z \, \Gamma_6, \tag{3.11b}$$

where

$$\Gamma_4 \equiv X_{203}, \quad \Gamma_5 \equiv X_{002}, \quad \Gamma_6 \equiv X_{323}. \tag{3.11c}$$

Here, $\mathscr{V}_{\boldsymbol{k}}^{\text{VB}}$ follows from replacing in $\mathscr{H}_{\boldsymbol{k}}^{\text{kin}}$ the Pauli matrices with index 1 by the Pauli matrices with index 2 and the cosine by the sine function. As it should be

$$\mathscr{V}_{-\boldsymbol{k}}^{\text{VB}*} = \mathscr{V}_{\boldsymbol{k}}^{\text{VB}}. \tag{3.12}$$

On the other hand, the cubic symmetry of $\mathscr{H}_{\boldsymbol{k}}^{\text{kin}}$ is reduced to an orthorhombic one for generic values of d_x, d_y, and d_z. Hereto, each member of the triplet of (dimer) masses $(\Gamma_4, \Gamma_5, \Gamma_6)$ anticommutes with each member of the triplet of Dirac matrices $(\Gamma_1, \Gamma_2, \Gamma_3)$. Thus, at the Dirac point (3.9), this dimerization pattern opens up the gap

$$2|\boldsymbol{d}| \equiv 2\sqrt{d_x^2 + d_y^2 + d_z^2}. \tag{3.13}$$

Among all 8×8 Hermitian matrices, there is one more matrix of the form (3.2a) that anticommutes with the three Dirac matrices (3.3a)–(3.5a) and the three dimerization mass matrices (3.11c). It is the diagonal matrix

$$\Gamma_7 := X_{333} \tag{3.14}$$

that represents a staggered chemical potential [a charge density wave with the momentum (π, π, π)]. We conclude that the most generic opening of a gap at the Dirac point (3.9) is encoded by the Hamiltonian

$$\mathscr{H}_{\boldsymbol{k}} := \mathscr{H}_{\boldsymbol{k}}^{\text{kin}} + \mathscr{V}_{\boldsymbol{k}}^{\text{VB}} + m X_{333} \tag{3.15a}$$

with the gap

$$\Delta \equiv 2\sqrt{d_x^2 + d_y^2 + d_z^2 + m^2} \tag{3.15b}$$

that depends on four real-valued parameters.

So far, we have been considering spinless fermions and we have assumed that the fermion number was a good quantum number. We attach to each spinless fermion a spin-$\frac{1}{2}$ degree of freedom, while preserving the conservation of the total fermion quantum number. We thus introduce the three Pauli matrices $\boldsymbol{\sigma} = (\sigma_1, \sigma_2, \sigma_3)$ and the 2×2 unit matrix σ_0. All four 2×2 matrices act on the spin-$\frac{1}{2}$ degrees of freedom. We also introduce the basis

$$X_{\mu_1\mu_2\mu_3\mu_4} := \sigma_{\mu_1} \otimes \tau_{\mu_2} \otimes \upsilon_{\mu_3} \otimes \zeta_{\mu_4} \tag{3.16}$$

with $\mu_1, \mu_2, \mu_3, \mu_4 = 0, 1, 2, 3$ for all 16×16 Hermitian matrices.

Define the 16×16 Hermitian matrices

$$\alpha_x \equiv -X_{0103}, \quad \alpha_y \equiv X_{0001}, \quad \alpha_z \equiv X_{0313}, \tag{3.17a}$$

$$\beta_x^{\text{VB}} \equiv X_{0203}, \quad \beta_y^{\text{VB}} \equiv X_{0002}, \quad \beta_z^{\text{VB}} \equiv X_{0323}, \tag{3.17b}$$

$$\beta_x^{\text{AF}} \equiv X_{1333}, \quad \beta_y^{\text{AF}} \equiv X_{2333}, \quad \beta_z^{\text{AF}} \equiv X_{3333}. \tag{3.17c}$$

All nine matrices are Hermitian, anticommute pairwise, and square to the identity 16×16 matrix. We then define the single-particle tight-binding model

$$\mathcal{H}_{\boldsymbol{k}} := \mathcal{H}_{\boldsymbol{k}}^{\text{kin}} + \mathcal{H}_{\boldsymbol{k}}^{\text{VB}} + \mathcal{H}_{\boldsymbol{k}}^{\text{AF}}, \tag{3.18a}$$

where

$$\mathcal{H}_{\boldsymbol{k}}^{\text{kin}} := \alpha_x \cos k_x + \alpha_y \cos k_y + \alpha_z \cos k_z, \tag{3.18b}$$

$$\mathcal{H}_{\boldsymbol{k}}^{\text{VB}} := \beta_x^{\text{VB}} d_x \sin k_x + \beta_y^{\text{VB}} d_y \sin k_y^{\text{VB}} + \beta_z^{\text{VB}} d_z \sin k_z, \tag{3.18c}$$

$$\mathcal{H}_{\boldsymbol{k}}^{\text{AF}} := \beta_x^{\text{AF}} n_x + \beta_y^{\text{AF}} n_y + \beta_z^{\text{AF}} n_z. \tag{3.18d}$$

Reversal of time is defined by conjugation with

$$\mathcal{T} := i X_{2000} \, \mathsf{K}, \tag{3.18e}$$

where K represents complex conjugation. Any nonvanishing value for any one of n_x, n_y, and n_z breaks time-reversal symmetry.

There are 16 bands that form an eightfold-degenerate valence band and an eightfold-degenerate conduction band. Conduction and valence bands are separated by the direct gap

$$\Delta \equiv 2\sqrt{\boldsymbol{d}^2 + \boldsymbol{n}^2} \tag{3.19a}$$

at the eight corners of the Brillouin zone. The gap at the Dirac point (3.9) thus depends on six real-valued parameters that can be interpreted as the pair of three-component vectors

$$\boldsymbol{d} := (d_x \; d_y \; d_z) \tag{3.19b}$$

and

$$\boldsymbol{n} := (n_x\ n_y\ n_z). \tag{3.19c}$$

The vector $\boldsymbol{d}$ realizes dimerization of the hopping amplitude within the repeat unit cell of Fig. 9. Using two different color codes to represent the sign of the dimerized hopping amplitude realizes a valence-bond covering of the cubic lattice by which each site is the end point of one and only one colored nearest-neighbor bond. The vector $\boldsymbol{n}$ realizes a collinear magnetic order with the antiferromagnetic wave vector (π, π, π) within the repeat unit cell of Fig. 9.

B. Dualities between point defects

We work with the single-particle tight-binding Hamiltonian (3.18) that we linearize about the Dirac point (3.9). The cubic lattice is thus replaced by Euclidean space $\mathbb{R}^3$, whose points we denote with $\boldsymbol{r} = (r_x, r_y, r_z)$. We consider static configurations of the vector fields $\boldsymbol{d}(\boldsymbol{r})$ and $\boldsymbol{n}(\boldsymbol{r})$ that support a monopole at the origin of $\mathbb{R}^3$.

For example, in the presence of one such defect, say in $\boldsymbol{d}$, the single-particle tight-binding Hamiltonian (3.18). is approximated to linear order in a gradient expansion around the Dirac point (3.9) by

$$\begin{aligned}\mathcal{H} := i\alpha_1\partial_x + i\alpha_2\partial_y + i\alpha_3\partial_z + f(\boldsymbol{r})\big[\hat{d}_x(\boldsymbol{r})\,\beta_x^{\mathrm{VB}} \\ + \hat{d}_y(\boldsymbol{r})\,\beta_y^{\mathrm{VB}} + \hat{d}_z(\boldsymbol{r})\,\beta_z^{\mathrm{VB}}\big],\end{aligned} \tag{3.20a}$$

where $f(\boldsymbol{r})$ is a smooth monotonic function satisfying

$$f(\boldsymbol{0}) = 0, \quad \lim_{|\boldsymbol{r}|\to\infty} f(\boldsymbol{r}) = 1, \tag{3.20b}$$

while the function $\hat{\boldsymbol{d}}$ is singular at the origin

$$\hat{\boldsymbol{d}}(\boldsymbol{r}) := \frac{\boldsymbol{r}}{|\boldsymbol{r}|} \tag{3.20c}$$

for $\boldsymbol{r} \in \mathbb{R}^3$. The singularity of $\boldsymbol{d}(\boldsymbol{r})$ has a topological character, for the order parameter $\boldsymbol{d}$ has the integer-valued winding number

$$W := \int_{\mathbb{R}^3} \frac{d^3\boldsymbol{r}}{8\pi}\frac{\partial}{\partial r_i}\left[\epsilon_{ijk}\,\epsilon_{abc}\,\hat{d}_a(\boldsymbol{r})\left(\frac{\partial \hat{d}_b}{\partial r_j}\right)(\boldsymbol{r})\left(\frac{\partial \hat{d}_c}{\partial r_k}\right)(\boldsymbol{r})\right] \tag{3.20d}$$

of magnitude one around the origin. The single-particle Hamiltonian (3.20a) obeys the index theorem (see Ref. [53] and, in a slightly more general context, Ref. [58])

$$\mathrm{Index}\,\mathcal{H} = W\,\mathrm{tr}\,\sigma_0 = 2W, \tag{3.20e}$$

where the left-hand side is the analytical index of $\mathcal{H}$ that counts the difference in the number of zero modes of $\mathcal{H}$ with the chiral eigenvalues ± 1, respectively, of a chiral operator that one may choose to be

$$\beta_z^{\mathrm{AF}} := X_{3333} \tag{3.20f}$$

without loss of generality.

If β_z^{AF} is used as a probe, i.e., as a small perturbation to the single-particle Hamiltonian (3.20a), it will lift the spin degeneracy of the zero modes through the Zeeman effect. Which of the spin projections acquires a positive energy depends on the eigenvalue of the chiral zero modes with respect to β_z^{AF}. In turn, the sign of this eigenvalue depends on which sublattice [even versus odd sites as measured by $(-1)^{i_x+i_y+i_z}$] the chiral zero modes is nonvanishing, i.e., on the sign of the winding number. Hence, the core of the monopole in the VBS order parameter $\boldsymbol{d}$ nucleates Neel order. The same argument can be reversed to infer that a monopole in the Neel order parameter $\boldsymbol{n}$ nucleates dimer order at its core.

C. Functional bosonization nonlinear sigma model with a Wess-Zumino term

We define the dimensionless vector field $\boldsymbol{N}(\tau, \boldsymbol{r}) \in \mathbb{R}^6$ comprised of the Neel, $\boldsymbol{n}(\tau, \boldsymbol{r}) \in \mathbb{R}^3$, and VBS (dimer), $\boldsymbol{d}(\tau, \boldsymbol{r}) \in \mathbb{R}^3$, order parameters through its components

$$\boldsymbol{N}(\tau, \boldsymbol{r}) \equiv (\boldsymbol{n}(\tau, \boldsymbol{r}), \boldsymbol{d}(\tau, \boldsymbol{r})), \tag{3.21a}$$

$$\boldsymbol{n}(\tau, \boldsymbol{r}) \equiv (n_x(\tau, \boldsymbol{r}), n_y(\tau, \boldsymbol{r}), n_z(\tau, \boldsymbol{r})), \tag{3.21b}$$

$$\boldsymbol{d}(\tau, \boldsymbol{r}) \equiv (d_x(\tau, \boldsymbol{r}), d_y(\tau, \boldsymbol{r}), d_z(\tau, \boldsymbol{r})). \tag{3.21c}$$

We define the single-particle Dirac Hamiltonian

$$\mathcal{H} := i\boldsymbol{\alpha}\cdot\boldsymbol{\partial} + m\,\boldsymbol{N}(\tau, \boldsymbol{r})\cdot\boldsymbol{\beta}, \tag{3.21d}$$

where the constant m has the dimension of inverse length

$$\boldsymbol{\alpha} := (\alpha_x, \alpha_y, \alpha_z) \tag{3.21e}$$

and

$$\boldsymbol{\beta} := \left(\beta_x^{\mathrm{AF}}, \beta_y^{\mathrm{AF}}, \beta_z^{\mathrm{AF}}, \beta_x^{\mathrm{VB}}, \beta_y^{\mathrm{VB}}, \beta_z^{\mathrm{VB}}\right). \tag{3.21f}$$

We define the four Hermitian 16×16 matrices

$$\begin{aligned}\gamma_0 &:= \beta_x^{\mathrm{AF}}, \quad \gamma_1 := i\beta_x^{\mathrm{AF}}\alpha_x, \\ \gamma_2 &:= i\beta_x^{\mathrm{AF}}\alpha_y, \quad \gamma_3 := i\beta_x^{\mathrm{AF}}\alpha_z,\end{aligned} \tag{3.21g}$$

together with the six 16×16 matrices

$$\begin{aligned}\Gamma_1 &:= \beta_x^{\mathrm{AF}}\beta_x^{\mathrm{AF}}, \quad \Gamma_4 := \beta_x^{\mathrm{AF}}\beta_x^{\mathrm{VB}}, \\ \Gamma_2 &:= \beta_x^{\mathrm{AF}}\beta_y^{\mathrm{AF}}, \quad \Gamma_5 := \beta_x^{\mathrm{AF}}\beta_y^{\mathrm{VB}}, \\ \Gamma_3 &:= \beta_x^{\mathrm{AF}}\beta_z^{\mathrm{AF}}, \quad \Gamma_6 := \beta_x^{\mathrm{AF}}\beta_z^{\mathrm{VB}}.\end{aligned} \tag{3.21h}$$

We define the partition function in $(3+1)$-dimensional Euclidean space-time to be

$$Z_{\mathrm{HS}} := \int \mathcal{D}[\boldsymbol{N}]\, e^{-\int d^4x\,\mathcal{L}_{\mathrm{HS}}} \int \mathcal{D}[\bar{\psi}, \psi]\, e^{-\int d^4x\,\mathcal{L}}, \tag{3.21i}$$

where

$$\mathcal{L}_{\mathrm{HS}} := \frac{1}{2}\int d^4x \left[\frac{\boldsymbol{n}^2(x)}{U_{\mathrm{AF}}} + \frac{\boldsymbol{d}^2(x)}{U_{\mathrm{VB}}}\right] \tag{3.21j}$$

and

$$\mathcal{L} := \bar{\psi}(x)\left[i\sum_{\mu=0}^{3}\gamma_\mu\frac{\partial}{\partial x_\mu} + im\sum_{a=1}^{6}N_a(x)\Gamma_a\right]\psi(x). \tag{3.21k}$$

Here, $U_{\mathrm{AF}} \geqslant 0$ and $U_{\mathrm{VB}} \geqslant 0$ are couplings with the dimension of length raised to the power $(d+1)$. Moreover, the 16 components of $\bar{\psi}(x)$ and the 16 components of $\psi(x)$ are Grassmann valued and independent. Each component depends on the position $x \equiv (x_\mu) := (\tau, \boldsymbol{r}) \in \mathbb{R}^4$ in $(3+1)$-dimensional

Euclidean space-time. If we integrate over the vector field (order parameter) $\boldsymbol{N}$ in the partition function, there follows the quartic contact fermionic interaction density

$$\frac{m^2 U_{\mathrm{AF}}}{2} \sum_{a=1}^{3} (\bar{\psi}\ \Gamma_a\, \psi)^2 + \frac{m^2 U_{\mathrm{VB}}}{2} \sum_{a=4}^{6} (\bar{\psi}\ \Gamma_a\, \psi)^2 = -\frac{m^2 U_{\mathrm{AF}}}{2} \sum_{a=1}^{3} \left(\psi^\dagger \beta_a^{\mathrm{AF}} \psi\right)^2 - \frac{m^2 U_{\mathrm{VB}}}{2} \sum_{a=1}^{3} \left(\psi^\dagger \beta_a^{\mathrm{VB}} \psi\right)^2, \tag{3.22a}$$

where

$$\bar{\psi} \equiv \psi^\dagger\, i\beta_x^{\mathrm{AF}}. \tag{3.22b}$$

When the fermionic quartic interaction in the channel $a = 1, \ldots, 6$ is expressed in terms of $(\psi^\dagger\, \beta_a\, \psi)^2$, it may be interpreted as an attractive interaction since $(\psi^\dagger\, \beta_a\, \psi)$, as an operator, is Hermitian so that its square can only have positive or vanishing eigenvalues.

Alternatively, we may also define the partition function

$$Z_{\mathrm{NLSM}} := \int \mathcal{D}[\boldsymbol{N}]\, \delta(\boldsymbol{N}^2 - 1) \int \mathcal{D}[\bar{\psi}, \psi]\, e^{-\int d^4x\, \mathcal{L}}. \tag{3.23}$$

As any $m \neq 0$ opens a spectral gap in the single-particle Dirac spectrum, we can integrate approximately the Grassmann fields within a gradient expansion. There follows the approximate bosonic partition function

$$Z_{\mathrm{NLSM}} \approx \int \mathcal{D}[\boldsymbol{N}]\, \delta(\boldsymbol{N}^2 - 1)\, e^{iS_{\mathrm{topo}}[\boldsymbol{N}]}\, e^{-\int d\tau \int d^3\boldsymbol{x}\, \mathcal{L}_{\mathrm{eff}}}. \tag{3.24a}$$

The Lagrangian density

$$\mathcal{L}_{\mathrm{eff}} := \frac{1}{2g} \sum_{\mu=0}^{3} (\partial_\mu \boldsymbol{N})^2, \quad x \equiv (\tau, \boldsymbol{x}) \equiv (x_\mu), \tag{3.24b}$$

in imaginary time $x_0 \equiv \tau := it$ is that of the nonlinear sigma model (NLSM) with the unit sphere $\mathsf{S}^{6-1} = \mathsf{S}^5$ as the target manifold. The bare coupling

$$g \propto m^{1-d} \tag{3.24c}$$

has the dimension

$$[g] = [\mathrm{length}]^{d-1} \tag{3.24d}$$

with $d = 3$. A necessary condition for the presence of the phase factor $\exp(iS_{\mathrm{topo}}[\boldsymbol{n}])$, *one that is compatible with locality*, is that the homotopy group

$$\pi_n(\mathsf{S}^5) \neq \emptyset \tag{3.24e}$$

is not trivial for one of the integers $n = 1, 2, \ldots, 5$ (the upper bound $5 = d + 2$ with $d = 3$ on n follows from demanding that the equations of motion for $\boldsymbol{N}$ are local). This condition is only met for $n = 5$.

Explicit computation (see Ref. [59] and references therein) yields the nonvanishing topological action given by

$$S_{\mathrm{topo}}[\boldsymbol{N}] = 2\pi\, S_{\mathrm{WZ}}[\boldsymbol{N}]. \tag{3.25a}$$

Here, $S_{\mathrm{WZ}}[\boldsymbol{N}]$ is the Wess-Zumino action, an action that is nonlocal in $(3+1)$-dimensional Euclidean space-time, but delivers local equations of motion. When Euclidean space-time $\mathbb{R}^{3+1}$ is compactified to S^{3+1}, the Wess-Zumino action is given by

$$S_{\mathrm{WZ}}[\boldsymbol{N}] = \frac{1}{(3+2)!\,\mathrm{Area}(\mathsf{S}^{3+2})} \int_0^1 du \int_{\mathsf{S}^{3+1}} d^{3+1}x \times \epsilon_{\mu_1 \ldots \mu_{3+2}}\, \epsilon_{a a_1 \ldots a_{3+2}}\, \bar{N}_a(u,x)\, \partial_{\mu_1} \bar{N}_{a_1}(u,x) \ldots \times \partial_{\mu_{3+2}} \bar{N}_{a_{3+2}}(u,x), \tag{3.25b}$$

whereby the vector field

$$\bar{\boldsymbol{N}}(u,x) = (\bar{N}_1(u,x), \ldots, \bar{N}_{3+2}(u,x), \bar{N}_{3+3}(u,x)) \tag{3.25c}$$

smoothly interpolates between

$$\bar{\boldsymbol{N}}(0,x) := (0, \ldots, 0, N_{3+3}(x)) \tag{3.25d}$$

and

$$\bar{\boldsymbol{N}}(1,x) := (N_1(x), \ldots, N_{3+2}(x), N_{3+3}(x)) \in \mathsf{S}^{3+2} \tag{3.25e}$$

as a function of $0 \leqslant u \leqslant 1$. The real-valued vector field $\bar{\boldsymbol{N}}(u,x)$ is therefore defined on a disk $D \subset \mathbb{R}^{3+2}$ such that its boundary is the compactified space-time S^{3+1}, i.e., $\partial D = \mathsf{S}^{3+1}$. The existence of the smooth vector field (3.25c) obeying conditions (3.25d) and (3.25e) is guaranteed from the identity $\pi_{3+1}(\mathsf{S}^{3+2}) = \emptyset$.

D. Phase diagrams

In this section, we discuss the phase diagrams of models (3.24) and (3.21), in this order. We then discuss the phase diagram of a cubic lattice model that realizes the π-flux phase in the noninteracting limit and, upon switching on local fermionic interactions with $\mathrm{O}(3) \times \mathrm{O}(3)$ symmetry, can be described by the effective field theory (3.21) in the low-energy limit.

With regard to the NLSM (3.24), we need to review the RG flow of NLSMs on Riemannian manifolds with positive curvature at zero temperature when space has dimension $d \geqslant 2$ (i.e., space-time has dimension greater than or equal to 3). In the absence of a topological term, there are two phases as shown in Fig. 10(a). (1) There is a long-range ordered phase with spontaneous breaking of a continuous symmetry when $g < g_{\mathrm{c}}$. (2) There is a symmetric quantum disordered gapped phase when $g > g_{\mathrm{c}}$. (3) The quantum critical point $g = g_{\mathrm{c}}$ realizes a continuous phase transition between these two phases of matter. Adding a topological term does not modify the perturbative RG flow when $g \lesssim g_{\mathrm{c}}$. However, it does change the nature of the fixed point of the RG flow when $g > g_{\mathrm{c}}$, as this fixed point now describes a symmetric gapless phase, as is indicated in Fig. 10(b).

With regard to the model (3.21), we conjecture that its phase diagram at zero temperature can be deduced from the phase diagram in Figs. 10(a) and 10(b) as follows. Let

$$\Delta U := \frac{U_{\mathrm{AF}} - U_{\mathrm{VB}}}{2} \tag{3.26a}$$

measure the anisotropy in the relative strength between the coupling $U_{\mathrm{AF}} \geqslant 0$ of the interaction favoring Neel order and the coupling $U_{\mathrm{VB}} \geqslant 0$ of the interaction favoring dimer order.

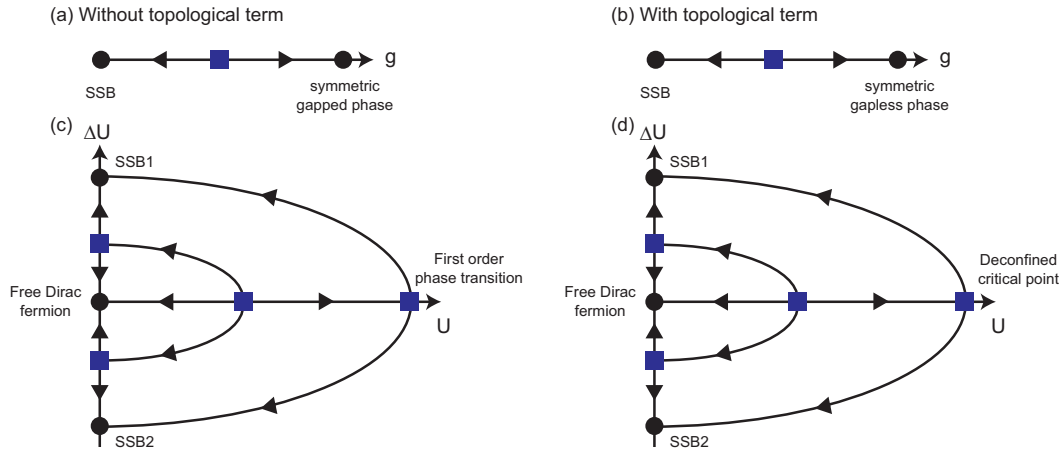

FIG. 10. Renormalization-group (RG) flows for the NLSM with O(6) symmetry in $(3+1)$-dimensional space-time (a) without any topological term and (b) with a Wess-Zumino term. (c), (d) Show RG flows for Dirac fermions perturbed by $O(3)\times O(3)$ symmetric interactions in $(3+1)$-dimensional space-time, assuming that bosonization in their Mott insulating phases delivers the RG flows in (a) and (b), respectively, when the interactions are fine tuned to an O(6) symmetric interaction.

We denote with

$$U := \frac{U_{\mathrm{AF}} + U_{\mathrm{VB}}}{2} \tag{3.26b}$$

the mean value of $U_{\mathrm{AF}} \geqslant 0$ and $U_{\mathrm{VB}} \geqslant 0$. The isotropic case is defined by

$$\Delta U = 0, \quad U = U_{\mathrm{AF}} = U_{\mathrm{VB}}. \tag{3.26c}$$

We consider the isotropic case (3.26c) first, in which case the $O(3)\times O(3)$ symmetry of the anisotropic quartic contact fermionic interaction (3.22a) becomes the O(6) symmetry of the isotropic contact fermionic interaction

$$\frac{m^2 U}{2}\sum_{a=1}^{6}(\bar{\psi}\,\Gamma_a\,\psi)^2 = -\frac{m^2 U}{2}\left[\sum_{a=1}^{3}\left(\psi^\dagger\beta_a^{\mathrm{AF}}\psi\right)^2 + \sum_{a=1}^{3}\left(\psi^\dagger\beta_a^{\mathrm{VB}}\psi\right)^2\right]. \tag{3.27}$$

Since any point-contact interaction for Dirac fermions at half-filling is irrelevant within perturbative RG when the dimensionality d of space is larger than one ($d > 1$), the ground state for small U is adiabatically connected to that in the noninteracting limit $U = 0$. Upon increasing the coupling U above some critical value U_{c}, a single-particle gap opens, long-range order is established, and the mapping to an effective NLSM becomes a good approximation at low energies. Since the bare coupling g in the NLSM and the bare fermionic coupling U have the relationship $g \sim U$, we expect a long-range ordered phase for intermediate values of U, and a symmetric phase for larger values of U that is either gapped in the absence of a topological term [Fig. 10(c) with $\Delta U = 0$] or gapless in the presence of a topological term [Fig. 10(d) with $\Delta U = 0$].

If we break the O(6) symmetry of the quartic interaction (3.27) by assuming that $\Delta U \neq 0$ in

$$U_{\mathrm{AF}} = U + \Delta U, \quad U_{\mathrm{VB}} = U - \Delta U, \tag{3.28}$$

we infer the phase diagrams in Figs. 10(c) and 10(d) depending on the absence or presence of dual topological point defects, respectively. Indeed, the choice $U \gtrsim U_{\mathrm{c}}$ with $\Delta U > 0$ selects the mean field order parameter $\bar{N} = (\bar{\boldsymbol{n}}, \bar{\boldsymbol{d}})$ aligned along the antiferromagnetic direction $(\bar{\boldsymbol{n}}, \boldsymbol{0})$. The choice $U \gtrsim U_{\mathrm{c}}$ with $\Delta U < 0$ selects the mean field order parameter $\bar{N} = (\bar{\boldsymbol{n}}, \bar{\boldsymbol{d}})$ aligned along the direction of $(\boldsymbol{0}, \bar{\boldsymbol{d}})$. These two ordered phases are separated by a first-order phase transition point in the NLSM perturbed by a symmetry-breaking term in the absence of a topological term as shown in Fig. 10(c) (we have ignored the case of a phase with coexisting orders for simplicity). However, in the presence of a topological term, the segment $U_{\mathrm{c}} < U < U_\star$ and $\Delta U = 0$ should instead be governed by a quantum critical point (which is a $d = 3$ analog of the deconfined quantum critical point proposed in Refs. [7–9] when $d = 2$) at $U = U_\star$ and $\Delta U = 0$ [see Fig. 10(d)].

The phase diagram of a local fermionic lattice regularization of the model (3.21) would then look as follows (see Fig. 11). When both U_{AF} and U_{VB} are small, fermionic interactions are irrelevant perturbations to the semimetallic phase (the noninteracting π-flux phase). When $U_{\mathrm{VB}} = 0$ while increasing $U_{\mathrm{AF}} > 0$ across the critical value $U_{\mathrm{AF}}^{\mathrm{c}} > 0$, the semimetallic phase is unstable to a Neel long-ranged ordered antiferromagnetic (Mott) insulating phase. When $U_{\mathrm{AF}} = 0$ while increasing U_{VB} across the critical value $U_{\mathrm{VB}}^{\mathrm{c}} > 0$, the semimetallic phase is unstable to a dimer long-ranged ordered (Mott) insulating phase. Now, the π-flux phase on the square lattice perturbed by local fermionic interactions with $O(3)\times O(2)$ symmetry shows the direct phase transition between Neel and dimer phases for sufficiently large $U_{\mathrm{AF}} = U_{\mathrm{VB}}$. This direct phase transition is governed by an unstable fixed point, namely, the fixed point of the NLSM with a topological term that describes a gapless symmetric phase with O(5) symmetry [10,11,29]. Similarly, one possible scenario for the π flux on the cubic lattice that is perturbed by local fermionic interactions with $O(3)\times O(3)$ symmetry is that the Neel and dimer phases are separated by a phase boundary that is governed by a single unstable fixed point, namely, the fixed point of the NLSM with a topological term that describes a gapless symmetric phase with O(6) symmetry, as is shown

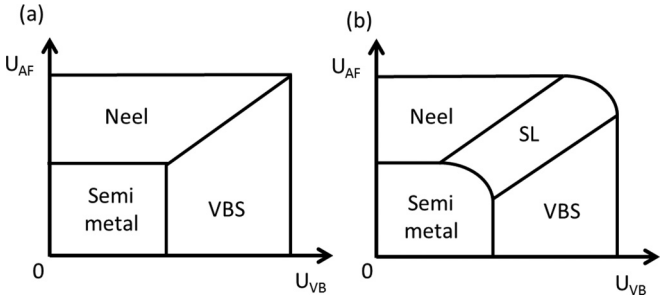

FIG. 11. Two possible phase diagrams for interacting fermionic tight-binding models at half-filling with an O(3) × O(3) symmetry that realize the π-flux phase on the cubic lattice in the noninteracting limit. (a) There exists a phase boundary between the Neel and dimer (valence bond solid) phases that is governed by a continuous quantum critical point at which the dual point defects of either phases have simultaneously proliferated. (b) The Neel and dimer (valence bond solid) phases do not touch. They are separated by a gapless spin-liquid (SL) phase characterized by the dual point defects of either phases being simultaneously deconfined.

in Fig. 11(a). However, working in $d = 3$ allows for another scenario that is shown in Fig. 11(b). In three-dimensional space, the antiferromagnetic and dimer dual point defects might be simultaneously deconfined in an extended region of coupling space instead of a single point in coupling space as is the case in two-dimensional space [26]. If so, a gapless spin-liquid (SL) phase, in which some putative matter fields are coupled to Abelian gauge fields in a Coulomb-type phase, could separate the Neel phase from the dimer long-range ordered phases.

IV. SUMMARY

The phase diagram at vanishing temperature of the quantum spin-$\frac{1}{2}$ antiferromagnetic J_1-J_2 XYZ chain was studied using both bosonization and numerical techniques. The symmetry group of the quantum spin-$\frac{1}{2}$ J_1-J_2 XYZ chain obeying periodic boundary conditions is generated by

$$\mathfrak{G} := R_\pi^\alpha \times R_\pi^\beta \times T \times P \times \Theta. \tag{4.1a}$$

Here, R_π^α and R_π^β denote any pair of distinct π rotations around the $\alpha \neq \beta = x, y, z$ axis in spin space, T denotes a translation by one lattice spacing, P denotes a site inversion, and Θ denotes reversal of time. It was shown that there are four gapped long-ranged ordered phases consisting of three Neel phases and one dimer phase. The corresponding patterns of spontaneous symmetry breaking (SSB) are

$$\mathfrak{G} \to \mathfrak{G}_{\mathrm{N}_\alpha} := R_\pi^\alpha \times P \times (T\,\Theta) \tag{4.1b}$$

for the Neel$_\alpha$ phase with $\alpha = x, y, z$ and

$$\mathfrak{G} \to \mathfrak{G}_{\mathrm{VBS}} := R_\pi^\alpha \times R_\pi^\beta \times \Theta \tag{4.1c}$$

for the dimer (VBS) phase. Because no pair of these residual symmetry groups obeys an ordering relation through the inclusion, Landau's theory of phase transitions precludes a direct continuous phase transition between any pair of these long-range ordered phases. Instead, Landau's theory of phase transitions predicts either coexistence or a direct first-order phase transition. Contrary to this expectation, we have shown that the three Neel phases and the dimer phase are separated from each other by six planes of phase boundaries realizing Gaussian criticality when $0 \leqslant J_2/J_1 < \frac{1}{2}$. We also have shown that each long-range ordered phase harbors topological point defects (domain walls) that are dual to those across the phase boundary in that a defect in one ordered phase locally binds the other type of order around its core. The Landau-forbidden continuous phase transitions are driven by the simultaneous proliferation (deconfinement) of these dual topological point-like defects.

We have also shown that a one-dimensional model of interacting fermions with a suitable choice of interactions can undergo a Landau-forbidden phase transition belonging to the same Gaussian universality class as those in the quantum spin-$\frac{1}{2}$ antiferromagnetic J_1-J_2 XYZ chain. Moreover, the mechanism at play here is not tied to the dimensionality of space. This observation led us to consider a tight-binding model on the cubic lattice that realizes a semimetallic phase in the noninteracting limit (the π-flux phase). Upon linearization of the noninteracting spectrum about the Fermi points (Dirac points) and the addition of interactions displaying an O(3) × O(3) symmetry in the continuum, sufficiently strong interactions can stabilize two Mott phases. One Mott phase supports collinear antiferromagnetic order. The other Mott phase supports dimer long-range order on the lattice. Both ordered phases were shown to support topological point defects, hedgehogs, that are dual to each other in that a defect in one ordered phase locally binds the other type of order around its core. When the bare interaction strengths are fine tuned so as to display the symmetry O(6) and assuming that the bare interactions select a Mott insulating phase with the pattern of symmetry breaking O(6) → O(5), functional bosonization yields a nonlinear sigma model augmented by a Wess-Zumino term. From this fact, we conjectured that the Mott insulating phases are either separated by a phase boundary governed by a quantum critical point or by a gapless spin-liquid phase, both displaying an O(6) symmetry and simultaneous proliferation of the dual hedgehogs. A lattice regularization of the fermionic field theory could be amenable to sign-free Monte Carlo simulations, as was done in Refs. [29,30] in two-dimensional space.

ACKNOWLEDGMENTS

A.F. was supported in part by JSPS KAKENHI Grant No. 15K05141. T.H. was supported by JSPS KAKENHI Grants No. 15K05198 and No. 17H02931. T.M. was supported by the Gordon and Betty Moore Foundation's EPiQS Initiative Theory Center Grant (to UC Berkeley), and the Quantum Materials program at Lawrence Berkeley National Laboratory (LBNL) funded by the US DOE under Contract No. DE-AC02-05CH11231.

APPENDIX: MORE ON NUMERICS

1. The critical coupling $\mathcal{J}_c(L)$

The finite-size critical couplings $\mathcal{J}_c(L)$, obtained from the position as a function of $0 \leqslant \mathcal{J} < \frac{1}{2}$ of the cusp singularity of $\Delta E_0(L)$ for given values of L, Δ_y, and Δ_z entering the

quantum spin-$\frac{1}{2}$ antiferromagnetic J_1-J_2 XYZ Hamiltonian (2.1a), is extrapolated to its thermodynamic limit

$$\mathcal{J}_c \equiv \lim_{L\to\infty} \mathcal{J}_c(L) \tag{A1a}$$

using the second-order polynomial in $1/L$ given by

$$\mathcal{J}_c(L) = \mathcal{J}_c + \frac{\alpha_1}{L} + \frac{\alpha_2}{L^2}. \tag{A1b}$$

The fitting was done using the values of $\mathcal{J}_c(L)$ for $L = 8, 10, \ldots, 20$ obtained from exact diagonalization as input and taking $\mathcal{J}_c$, α_1, and α_2 as free parameters. Figure 12 shows the results for $\Delta_z = 2.0$ and $\Delta_y = 0.5$. The errors in $\mathcal{J}_c$ are estimated from the difference between the extrapolated value and $\mathcal{J}_c(L = 20)$. They are less than 0.4% of $\mathcal{J}_c$. Incidentally, the coefficient α_1 is much smaller than $\mathcal{J}_c$ and α_2 for all the cases calculated: α_1 is of the order 10^{-3} while $\mathcal{J}_c$ and α_2 are of the order 10^{-1}. This suggests that $\alpha_1 = 0$ as was already found for the quantum spin-$\frac{1}{2}$ antiferromagnetic J_1-J_2 XXZ chain [38].

2. DMRG

We performed the DMRG calculations for open chains hosting up to $L = 192$ spins (L is chosen a multiple of four). The maximum number of the states that were kept was $\chi = 160$. We checked that the average of the weight of discarded states at each step over the final DMRG sweep was smaller than 6×10^{-11}. We thereby confirmed that the DMRG data are accurate enough for our analysis.

3. Entanglement entropy

We consider an open chain made hosting L spins with L being a multiple of four. Let $l \geqslant 1$ be an integer smaller than L. The entanglement entropy $\mathcal{S}(l)$ is defined by

$$\mathcal{S}(l) := -\sum_j \rho_l(j) \ln \rho_l(j), \tag{A2}$$

where $\rho_l(j)$ is the jth eigenvalue of the subdensity matrix for the left l-site block in the ground state of the full open chain. As seen from Fig. 6, $\mathcal{S}(l)$ contains a sizable oscillating component that arises from the use of open boundary conditions. It was found numerically [51,52] that the oscillating contribution to the entanglement entropy $\mathcal{S}(l)$ that originates from choosing open boundary conditions is proportional to the oscillating component of the local bond-energy expectation value

$$E_{\rm osc}(l) := E_{\rm bond}(l) - E_{\rm uni}, \tag{A3a}$$

with

$$\begin{aligned} E_{\rm bond}(l) := J_1 \big\langle \big(S^x_l S^x_{l+1} + \Delta_y S^y_l S^y_{l+1} + \Delta_z S^z_l S^z_{l+1}\big)\big\rangle_L \\ + \frac{J_2}{2}\big\langle \big(S^x_{l-1} S^x_{l+1} + \Delta_y S^y_{l-1} S^y_{l+1} + \Delta_z S^z_{l-1} S^z_{l+1} \\ + S^x_l S^x_{l+2} + \Delta_y S^y_l S^y_{l+2} + \Delta_z S^z_l S^z_{l+2}\big)\big\rangle_L. \end{aligned} \tag{A3b}$$

The oscillating component $E_{\rm osc}(l)$ enters $\mathcal{S}(l)$ through

$$\mathcal{S}(l) = \frac{c}{6} \ln\left[f\left(l + \frac{1}{2}\right)\right] + \alpha_{\rm osc} E_{\rm osc}(l) + \mathcal{S}_0. \tag{A3c}$$

We have computed the local bond-energy expectation value $E_{\rm bond}(l)$ as well as the entanglement entropy $\mathcal{S}(l)$ using the DMRG method and obtained $E_{\rm osc}(l)$ by subtracting

$$E_{\rm uni} := \frac{1}{2}\left[E_{\rm bond}\left(\frac{L}{2}\right) + E_{\rm bond}\left(\frac{L}{2} + 1\right)\right] \tag{A3d}$$

from $E_{\rm bond}(l)$. Then, we have performed the least-square fitting of the data of $\mathcal{S}(l)$ and $E_{\rm osc}(l)$ to Eq. (A3c) taking c, $\alpha_{\rm osc}$, and $\mathcal{S}_0$ as fitting parameters. The data around the center of an open chain (for $3L/8 \leqslant l \leqslant 5L/8$) were used in the fitting. We thereby determine the central charge c.

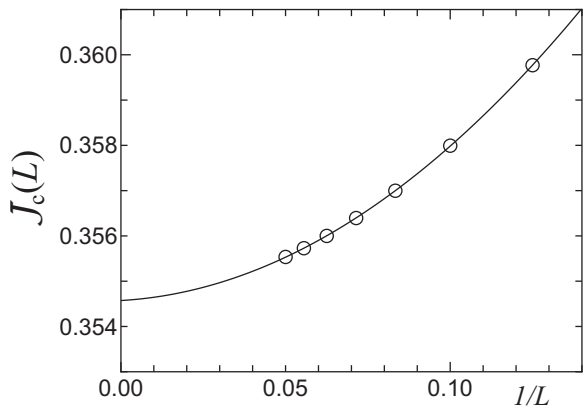

FIG. 12. Extrapolation of the critical coupling $\mathcal{J}_c(L)$ to its limit $\mathcal{J}_c$ when $L \to \infty$ for $\Delta_z = 2.0$ and $\Delta_y = 0.5$.

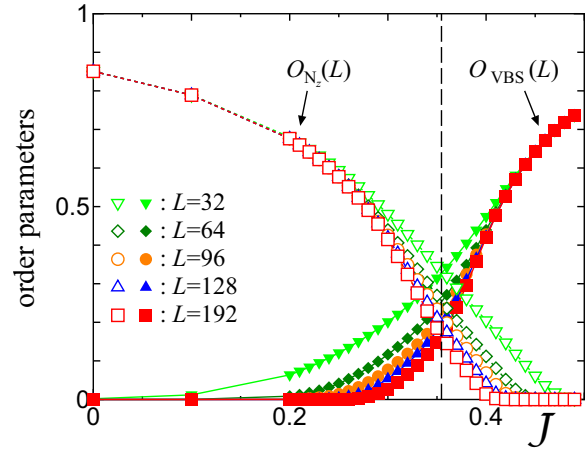

FIG. 13. Order parameters $O_{N_z}(L)$ (unfilled symbols) and $O_{\rm VBS}(L)$ (filled symbols) for $\Delta_z = 2.0$ and $\Delta_y = 0.5$ as functions of $\mathcal{J}$.

4. Long-range order from DMRG

We have measured the dimer and Neel$_z$ order parameters using the DMRG method on each side of a continuous quantum critical point reached by moving away from the value $\mathcal{J}_c$ holding the anisotropies Δ_y and Δ_z fixed. Here, $\mathcal{J}_c$ was identified by using methods based on exact diagonalization.

With regard to the dimer order, we calculated the local order parameter $O_{\rm VBS}(L)$ defined in Eq. (2.48). Whereas the

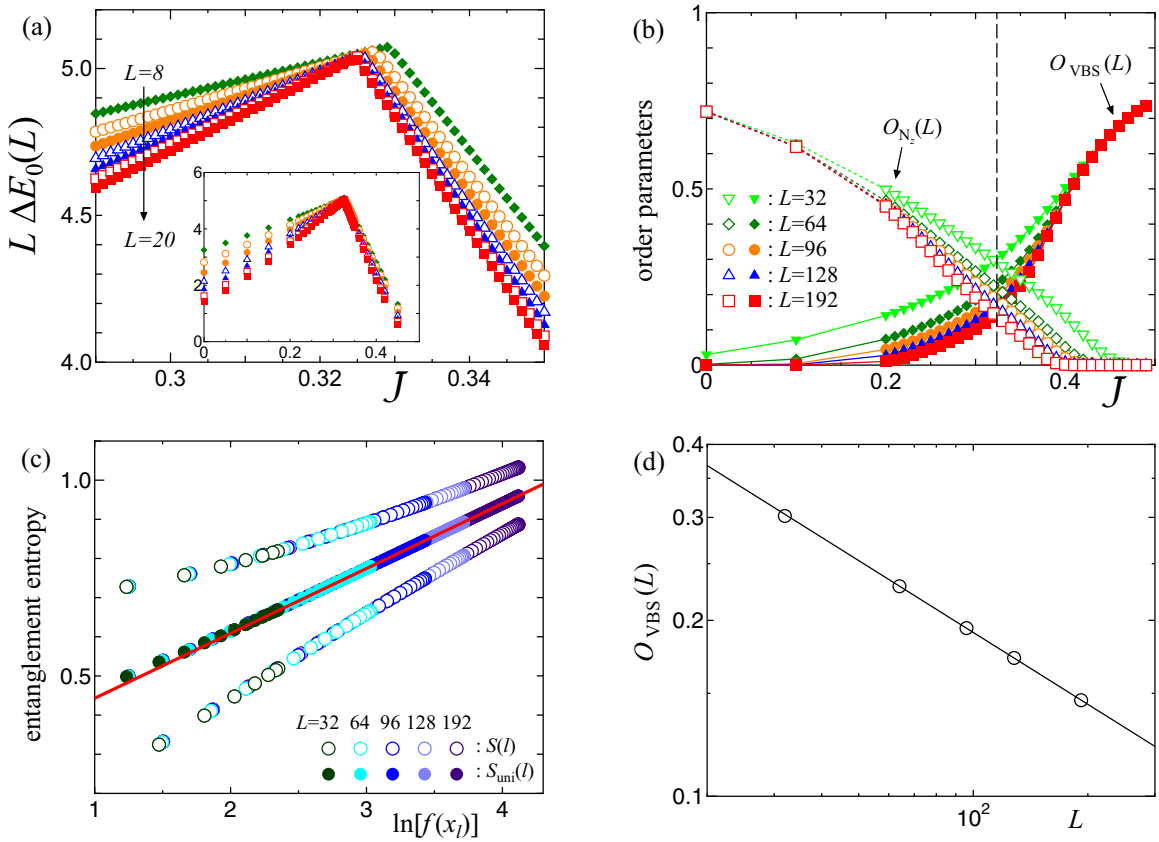

FIG. 14. Panels (a), (b), (c), and (d) are the counterparts to Figs. 5(a), 13, 6(b), and 7(a), respectively, when $\Delta_z = 3.0$ and $\Delta_y = 2.0$. The central charge c obtained in (c) (using the data for $L = 192$) is $c = 0.994$, and the exponent η obtained in (d) is $\eta = 1.22$.

two inequivalent dimer states are degenerate for finite chains hosting an even number of spins and obeying periodic boundary conditions, this is not true anymore when these chains obey open boundary conditions, as translation symmetry is broken by the two boundaries.

With regard to the Neel$_z$ order, the choice of open boundary conditions for a chain hosting an even number of spins is compatible with reversal of time, the operation that exchanges the two inequivalent classical Neel$_z$ states. Hence, no spontaneous symmetry breaking of time-reversal symmetry occurs for a chain hosting a finite and even number of spins. In order to detect numerically Neel$_z$ order, we added to Hamiltonian (2.1a) a symmetry-breaking term by coupling the first and last spins to a staggered magnetic field, i.e., we added to Hamiltonian (2.1a) the boundary energy cost

$$\mathcal{H}_h := -h\left[S^z_1 - (-1)^L S^z_L\right] \tag{A4}$$

with $h = 100\,J_1$. By design, $\mathcal{H}_h$ lifts the degeneracy of the classical Neel$_z$ states. We then calculated the local Neel$_z$-order parameter $O_{N_z}(L)$ defined by

$$O_{N_z}(L) := \left\langle \left(S^z_{\frac{L}{2}+1} - S^z_{\frac{L}{2}}\right)\right\rangle_L. \tag{A5}$$

We note that $\mathcal{H}_h$ is added only when we compute $O_{N_z}(L)$. We set $h = 0$ for all other observables.

Figure 13 shows the dependence on $\mathcal{J}$ of the Neel$_z$ order parameter $O_{N_z}(L)$ and of the dimer order parameter $O_{\rm VBS}(L)$ for $\Delta_z = 2.0$, $\Delta_y = 0.5$, and given L. These data suggest that the model exhibits the Neel$_z$ long-range order for $\mathcal{J} < \mathcal{J}_c$ and the dimer long-range order for $\mathcal{J} > \mathcal{J}_c$. We have performed the same analysis along all one-dimensional cuts with $\Delta_z = 2.0$ and the values of Δ_y given in Fig. 5(b) for which a putative Neel$_z$ long-range ordered phase is separated from a putative dimer long-range ordered phase by a continuous quantum critical point $\mathcal{J}_c$ as determined by exact diagonalization techniques. For all cases, the long-range ordered phases are the Neel$_z$ and dimer phases.

5. Scaling exponent η at quantum criticality

In order to estimate the exponent η at the Neel$_z$-dimer transition, we make the scaling ansatz

$$O_{\rm VBS}(L) = A\,L^{-\frac{1}{2\eta}} \tag{A6}$$

taking η and A as fitting parameters. The estimate of η was obtained from the fitting using the data of $O_{\rm VBS}(L)$ for $64 \leqslant L \leqslant 192$ while the error in η was determined by the difference between the estimate and η obtained using the data for $32 \leqslant L \leqslant 192$.

6. Complementary cuts

We have repeated our numerical analysis along the one-dimensional cuts (2.46) with Δ_y given in Fig. 5(b) for the three

one-dimensional cuts

$$\Delta_z = 3.0, \quad \Delta_y = 0.0, \quad 0 \leqslant \mathcal{J} < 0.5, \tag{A7a}$$
$$\Delta_z = 3.0, \quad \Delta_y = 0.5, \quad 0 \leqslant \mathcal{J} < 0.5, \tag{A7b}$$
$$\Delta_z = 3.0, \quad \Delta_y = 2.0, \quad 0 \leqslant \mathcal{J} < 0.5. \tag{A7c}$$

Figure 14 shows the numerical data along the one-dimensional cut (A7c). Hereto, the existence of a continuous quantum critical point with central charge $c = 1$ separating the Neel$_z$ phase from the dimer phase is confirmed. The same is true for the one-dimensional cuts (A7a) and (A7b).

[1] V. L. Berezinskiĭ, Zh. Eksp. Teor. Fiz. **59**, 907 (1970) [Sov. J. Exp. Theor. Phys. **32**, 493 (1971)].
[2] V. L. Berezinskiĭ, Zh. Eksp. Teor. Fiz. **61**, 1144 (1971) [Sov. J. Exp. Theor. Phys. **34**, 610 (1972)].
[3] J. M. Kosterlitz and D. J. Thouless, J. Phys. C: Solid State Phys. **6**, 1181 (1973).
[4] J. M. Kosterlitz, J. Phys. C: Solid State Phys. **7**, 1046 (1974).
[5] F. D. M. Haldane, Phys. Rev. Lett. **61**, 1029 (1988).
[6] N. Read and S. Sachdev, Phys. Rev. Lett. **62**, 1694 (1989).
[7] T. Senthil, A. Vishwanath, L. Balents, S. Sachdev, and M. P. A. Fisher, Science **303**, 1490 (2004).
[8] T. Senthil, L. Balents, S. Sachdev, A. Vishwanath, and M. P. A. Fisher, Phys. Rev. B **70**, 144407 (2004).
[9] M. Levin and T. Senthil, Phys. Rev. B **70**, 220403(R) (2004).
[10] A. Tanaka and X. Hu, Phys. Rev. Lett. **95**, 036402 (2005).
[11] T. Senthil and M. P. A. Fisher, Phys. Rev. B **74**, 064405 (2006).
[12] A. W. Sandvik, Phys. Rev. Lett. **98**, 227202 (2007).
[13] R. G. Melko and R. K. Kaul, Phys. Rev. Lett. **100**, 017203 (2008).
[14] F.-J. Jiang, M. Nyfeler, S. Chandrasekharan, and U.-J. Wiese, J. Stat. Mech. (2008) P02009.
[15] A. B. Kuklov, M. Matsumoto, N. V. Prokofev, B. V. Svistunov, and M. Troyer, Phys. Rev. Lett. **101**, 050405 (2008).
[16] J. Lou, A. W. Sandvik, and N. Kawashima, Phys. Rev. B **80**, 180414(R) (2009).
[17] A. W. Sandvik, Phys. Rev. Lett. **104**, 177201 (2010).
[18] A. Sen and A. W. Sandvik, Phys. Rev. B **82**, 174428 (2010).
[19] A. Banerjee, K. Damle, and F. Alet, Phys. Rev. B **82**, 155139 (2010).
[20] A. Banerjee, K. Damle, and A. Paramekanti, Phys. Rev. B **83**, 134419 (2011).
[21] A. Nahum, J. T. Chalker, P. Serna, M. Ortuño, and A. M. Somoza, Phys. Rev. X **5**, 041048 (2015).
[22] S. Pujari, F. Alet, and K. Damle, Phys. Rev. B **91**, 104411 (2015).
[23] S. Gazit, F. F. Assaad, S. Sachdev, A. Vishwanath, and C. Wang, Proc. Natl. Acad. Sci. USA **115**, E6987 (2018).
[24] X.-F. Zhang, Y.-C. He, S. Eggert, R. Moessner, and F. Pollmann, Phys. Rev. Lett. **120**, 115702 (2018).
[25] S. Ryu, C. Mudry, C.-Y. Hou, and C. Chamon, Phys. Rev. B **80**, 205319 (2009).
[26] P. Hosur, S. Ryu, and A. Vishwanath, Phys. Rev. B **81**, 045120 (2010).
[27] P. Ghaemi, S. Ryu, and D.-H. Lee, Phys. Rev. B **81**, 081403(R) (2010).
[28] P. Ghaemi and S. Ryu, Phys. Rev. B **85**, 075111 (2012).
[29] T. Sato, M. Hohenadler, and F. F. Assaad, Phys. Rev. Lett. **119**, 197203 (2017).
[30] Y. Liu, Z. Wang, T. Sato, M. Hohenadler, C. Wang, W. Guo, and F. F. Assaad, arXiv:1811.02583 (2018).
[31] Y.-Z. You, Y.-C. He, C. Xu, and A. Vishwanath, Phys. Rev. X **8**, 011026 (2018).
[32] M. A. Metlitski and R. Thorngren, Phys. Rev. B **98**, 085140 (2018).
[33] Z. Bi and T. Senthil, arXiv:1808.07465.
[34] Z. Wan and J. Wang, Phys. Rev. D **99**, 065013 (2019).
[35] S. Jiang and O. Motrunich, Phys. Rev. B **99**, 075103 (2019).
[36] H.-Z. Xu, S.-Y. Zhang, G.-C. Guo, and M. Gong, arXiv:1806.05814.
[37] K. Okamoto and K. Nomura, Phys. Lett. A **169**, 433 (1992).
[38] K. Nomura and K. Okamoto, J. Phys. A: Math. Gen. **27**, 5773 (1994).
[39] F. D. M. Haldane, Phys. Rev. B **25**, 4925 (1982).
[40] F. D. M. Haldane, Phys. Rev. B **26**, 5257 (1982).
[41] S. R. White and I. Affleck, Phys. Rev. B **54**, 9862 (1996).
[42] S. Eggert, Phys. Rev. B **54**, R9612 (1996).
[43] S. Furukawa, M. Sato, and A. Furusaki, Phys. Rev. B **81**, 094430 (2010).
[44] S. Furukawa, M. Sato, S. Onoda, and A. Furusaki, Phys. Rev. B **86**, 094417 (2012).
[45] T. Hikihara, A. Furusaki, and S. Lukyanov, Phys. Rev. B **96**, 134429 (2017).
[46] P. Lecheminant, A. O. Gogolin, and A. A. Nersesyan, Nucl. Phys. B **639**, 502 (2002).
[47] A. O. Gogolin, A. A. Nersesian, and A. M. Tsvelik, *Bosonization and Strongly Correlated Systems* (Cambridge University Press, 1998).
[48] C. Holzhey, F. Larsen, and F. Wilczek, Nucl. Phys. B **424**, 443 (1994).
[49] G. Vidal, J. I. Latorre, E. Rico, and A. Kitaev, Phys. Rev. Lett. **90**, 227902 (2003).
[50] P. Calabrese and J. Cardy, J. Stat. Mech. (2004) P06002.
[51] N. Laflorencie, E. S. Sørensen, M.-S. Chang, and I. Affleck, Phys. Rev. Lett. **96**, 100603 (2006).
[52] I. Affleck, N. Laflorencie, and E. S. Sørensen, J. Phys. A: Math. Theor. **42**, 504009 (2009).
[53] R. Jackiw and C. Rebbi, Phys. Rev. D **13**, 3398 (1976).
[54] J. V. José, L. P. Kadanoff, S. Kirkpatrick, and D. R. Nelson, Phys. Rev. B **16**, 1217 (1977).
[55] P. B. Wiegmann, J. Phys. C: Solid State Phys. **11**, 1583 (1978).
[56] The same action was obtained in Appendix E of Ref. [35] in the limit when $\Delta_y = 0$.
[57] C. Mudry, A. Furusaki, T. Morimoto, and T. Hikihara (unpublished).
[58] Y. Nishida, L. Santos, and C. Chamon, Phys. Rev. B **82**, 144513 (2010).
[59] A. Abanov and P. Wiegmann, Nucl. Phys. B **570**, 685 (2000).